Non-equilibrium phase transitions and critical phenomena in gauge/gravity duality

Masataka Matsumoto

A thesis presented for the degree of
Doctor of Philosophy

Department of Physics
Chuo University
Japan

Abstract

The non-equilibrium process is generally found in almost all systems in nature. Nevertheless, the understanding of universal properties in non-equilibrium systems is still lacking in contrast to equilibrium systems and a systematical approach has not yet been established. In this thesis, our primary purpose is to investigate some universal properties of non-equilibrium systems. In order to do this, we focus on non-equilibrium phase transitions and critical phenomena in a system of a non-equilibrium steady state. As seen in equilibrium phase transitions, it has been known that the system exhibits universal behaviors in critical phenomena of non-equilibrium phase transitions.

In this thesis, we study non-equilibrium phase transitions and critical phenomena within the framework of the gauge/gravity duality. The gauge/gravity duality has been proposed as a duality between a strongly coupled gauge field theory and the gravity theory in the context of the superstring theory. This duality enables us to analyze the non-equilibrium steady state beyond the linear response regime.

We analyze critical phenomena in a current-driven system, which undergoes non-equilibrium phase transitions. We define a susceptibility as the variation of order parameter with respect to the current density. We also find that the critical exponents agree with those of the Landau theory.

Moreover, we also analyze another non-equilibrium phase transition, which is associated with spontaneous symmetry breaking of the $U(1)$ chiral symmetry. We discover the novel tricritical point that appears only in the non-equilibrium steady state. We also find that critical exponents agree with those of the Landau theory.

Our findings imply that the non-equilibrium phase transitions in our setup are described by a Landau-like phenomenological theory. We hope that our results provide some clues to reveal the universal properties of non-equilibrium steady states.

Acknowledgement

Firstly, I would like to express my sincere gratitude to my supervisor Prof. Shin Nakamura for the continuous support of my Ph.D. research and related research, for his patience, motivation, and immense knowledge. His guidance helped me in all the time of research and writing of this thesis.

Besides my advisor, I am grateful to the rest of my thesis committee: Prof. Shunji Tsuchiya, Prof. Kenji Yonemitsu, Prof. Kotaro Tsugawa, and Prof. Satoshi Iso, for their insightful comments and encouragement, but also for the hard questions which incented me to widen my research from various perspectives.

I would like to thank my co-authors: Prof. Ryosuke Yoshii and Mr. Takuya Imaizumi for their collaborative efforts.

My sincere thanks also go to Prof. Shunichiro Kinoshita, Dr. Hironori Hoshino, Dr. Tomoya Hayata and Dr. Yuichi Fukazawa, who provides me the helpful discussions and comments for my thesis. Without their precious support, it would not be possible to conduct this research.

I am thankful to the group members for the stimulating discussions, for the sleepless nights we were working together before deadlines, and for all the fun we have had in the last four years.

Last but not the least, I would like to thank my family: my parents and to my brother and sister for supporting me spiritually throughout writing this thesis and my life in general.

Contents

Chapter 1

Introduction

Non-equilibrium phenomena have wider variety compared to equilibrium phenomena. In nature, most phenomena are far away from equilibrium. However, the theoretical understanding of the non-equilibrium process is still lacking in contrast to equilibrium statistical mechanics. The construction of non-equilibrium statistical mechanics or the understanding of the fundamental principle in non-equilibrium is a great challenge for modern theoretical physics. For example, the non-equilibrium steady state (NESS) is a simple extension of the equilibrium state, which can be considered as a rather special case of the class of steady states. In the NESS, there is no time variation of physical quantities, but entropy production and some flows are non-zero. Nevertheless, it has not been known whether a thermodynamic description of systems in a NESS exists.

As in equilibrium states, non-equilibrium phenomena are of particular interest if the system exhibits a phase transition. It has been known that a large variety of phenomenological non-equilibrium phase transitions appear in nature, for example, the absorbing-state transitions, the morphological transitions of growing surface, and so on (for example, see Ref. [1, 2] for reviews). The *universality*, which has been successful in equilibrium critical phenomena, can be applied to non-equilibrium critical phenomena as well. It has been known that there are various *non-equilibrium universality class*. However, it is expected that the universality of non-equilibrium critical phenomena has a wide variety since the non-equilibrium systems have more control parameters than those of the equilibrium systems. Therefore, further studies are required to find out some universal properties of non-equilibrium systems.

The aim of this thesis is primarily to investigate non-equilibrium phase

transitions and critical phenomena by using the *gauge/gravity duality*[1]. The gauge/gravity duality is a duality between a gravity theory and a strongly coupled quantum gauge field theory [3, 4, 5], which has been proposed in the framework of the superstring theory. The gauge/gravity duality provides a computational method for the strongly coupled gauge field theory in terms of general relativity. Up to now, there are vast applications of the gauge/gravity duality into several areas of physics such as condensed matter physics, quantum information, quantum chromodynamics (QCD), and so on (for example, see Refs. [6, 7, 8, 9]). In this thesis, we will particularly focus on the non-equilibrium phenomena of the strongly coupled gauge field theory that is realized by the gauge/gravity duality, which enables us to analyze the NESS regime beyond the linear response theory.

This thesis is organized as follows. In Chapter 2, we present a review of critical phenomena in equilibrium phase transitions. These fundamental properties are important in later results. In Chapter 3, we devote to review the idea and applications of the gauge/gravity duality. Chapter 4 is the main part in this thesis. This part is separated into two bodies. One is the computation of the critical exponents in the non-equilibrium phase transitions. These results are based on our published paper [10]. The other part is the analysis of the spontaneous symmetry breaking associated with the non-equilibrium phase transitions. This part is based on our work [11]. In Chapter 5, we present summary and future perspectives of this thesis.

[1] A review on application of the gauge/gravity duality to non-equilibrium physics is Ref. [12].

Chapter 2

Critical Phenomena

In this chapter, we present a brief review of critical phenomena in equilibrium phase transitions. In Sec. 2.1, we explain the general and phenomenological theory of equilibrium phase transitions, which is the so-called Landau theory. Some results in the Landau theory agree with critical phenomena in our non-equilibrium phase transitions as we discuss later. In Sec. 2.2, we introduce the tricritical point in equilibrium phase transitions. The tricritical point is a special point where the three-phase coexistence terminates. In Sec. 2.3, we analyze the behavior of the correlation function near the critical point by extending the Landau theory. It is shown that a certain correlation function also captures the universal properties of critical phenomena. In Sec. 2.4, we introduce dynamical critical phenomena, which characterize critical behaviors of the non-equilibrium state near the critical point.

2.1 Landau Theory

In this section, we will briefly review the Landau theory for equilibrium phase transitions. The Landau theory is based on rather general considerations of symmetry and analyticity. Nevertheless, this theory provides us crucial insights into phase transitions. It has been known that the Landau theory is a phenomenological model that corresponds to the mean-field theory and is derived from the microscopic model with the mean-field approximation.

Here we consider an example of a phase transition of ferromagnets. In this case, the order parameter and the external field corresponds to the magnetization and the external magnetic field, respectively. In the Landau theory, we assume the free energy to be an even function of the magnetization because of the symmetry under the spin-flip which stems from the time-

reversal symmetry. Since we are interested in the vicinity of the critical point, we assume that the magnetization is sufficiently small. Then we can expand the free energy as a power series in the magnetization up to the fourth power and ignore the higher-order terms:

$$F(M) = F_0 + aM^2 + bM^4, \tag{2.1}$$

where M is the magnetization. F_0 is a constant and we assume that b is a positive constant here, whereas $a = k(T - T_c)/T_c$ with a positive constant k. T_c is the critical temperature of the second-order phase transition.

Since a thermal equilibrium state is realized as a minimum of the free energy, the following equation determines the thermal equilibrium magnetization M_0

$$\left.\frac{\partial F(M)}{\partial M}\right|_{M_0} = 2aM_0 + 4bM_0^3 = 0 \tag{2.2}$$

Thus, $M_0 = 0$ for $T > T_c$ and

$$M_0 = \sqrt{-\frac{a}{2b}} = \sqrt{\frac{k(T_c - T)}{2bT_c}}, \tag{2.3}$$

for $T < T_c$. This result describes the appearance of the magnetization and thus exhibits the spontaneous symmetry breaking below T_c. If there is an external magnetic field in this system, the free energy is written as

$$F(M) = F_0 + aM^2 + bM^4 - HM, \tag{2.4}$$

where H is the external magnetic field. Then, the thermal equilibrium state is determined by the following relation:

$$\left.\frac{\partial F(M)}{\partial M}\right|_{M_0} = 2aM_0 + 4bM_0^3 - H = 0. \tag{2.5}$$

Although the solution of Eq. (2.5) is complicated, M_0 becomes simple for $T = T_c$:

$$M_0 = \left(\frac{H}{4b}\right)^{\frac{1}{3}}. \tag{2.6}$$

The magnetic susceptibility is defined as $\chi = \partial M/\partial H$. We obtain this from Eq. (2.5) as

$$\chi = \frac{1}{2a + 12bM^2}. \tag{2.7}$$

For $T > T_c$ with $M = 0$, we have

$$\chi = \frac{1}{2a} = \frac{T_c}{2k(T - T_c)} \equiv \chi_{T>T_c}, \tag{2.8}$$

whereas

$$\chi = \frac{1}{2a + 12b(-a/2b)} = \frac{T_c}{4k(T_c - T)} \equiv \chi_{T<T_c}, \tag{2.9}$$

for $T < T_c$. From Eqs. (2.8) and (2.9), the ratio of the coefficients of $|T - T_c|$, which is called as *critical amplitude ratio*, becomes two: $\chi_{T>T_c}/\chi_{T<T_c} = 2$. It should be emphasized that this value is universal in the sense that it does not depend on the specific values of k and T_c which reflect the depending on the microscopic parameters of the specific system. Thus it is tremendously important to determine such universal values since the critical phenomena for huge numbers of systems in the same universality class can be understood once those values are obtained.

Let us derive the specific heat from the free energy. The specific heat is defined by $C_v = -T\partial^2 F(M_0)/\partial T^2$. For $T < T_c$ and $H = 0$,

$$F(M_0) = F_0 + aM_0^2 + bM_0^4 = F_0 - \frac{k^2(T - T_c)^2}{4bT_c^2}. \tag{2.10}$$

Thus, we find that the specific heat is constant.

The characteristic behaviors of various quantities at the critical point are characterized by the *critical exponents*. The definitions of the critical exponents in ferromagnets are given by

$$M_0 \propto |T - T_c|^{\beta} \qquad (T < T_c), \tag{2.11}$$

$$M_0 \propto |H|^{1/\delta} \qquad (T = T_c), \tag{2.12}$$

$$\chi \propto |T - T_c|^{-\gamma} \qquad (T < T_c), \tag{2.13}$$

$$\chi \propto |T - T_c|^{-\gamma'} \qquad (T > T_c), \tag{2.14}$$

$$C_v \propto |T - T_c|^{-\alpha} \qquad (T < T_c). \tag{2.15}$$

In the Landau theory, the critical exponents are determined by Eqs. (2.3), (2.6), (2.8), (2.9), and (2.10) as:

$$\beta = \frac{1}{2}, \quad \delta = 3, \quad \gamma = \gamma' = 1, \quad \alpha = 0, \tag{2.16}$$

and these values are the same as those in the mean-field theory. Note that there are further two critical exponents η and ν, which are related to the behavior of correlation functions near the critical point as we will introduce later.

2.2 Tricritical point

A tricritical point is defined as the point in the phase diagram at which three-phase coexistence terminates. In this section, we derive the tricritical point from the Landau theory and review the difference compared to the critical point.

Hitherto we have assumed that the coefficient of the quartic term b to be positive. However, if b becomes negative, the free energy does not minima for finite M. Thus, one needs to consider the expansion of the Landau free energy up to the sixth power of the order parameter.

$$F(M) = F_0 + aM^2 + bM^4 + cM^6, \tag{2.17}$$

where c is a positive constant. In this case, c must be a positive constant since the free energy must maintain stability. If $b > 0$, the sixth power term is just a correction to results of the previous section and it does not change critical phenomena. If $b < 0$, however, it turns out that results are qualitatively different.

Assuming that $b < 0$ and $c > 0$, we consider the a dependence of the free energy. A minimum of the free energy is determined by the following equation

$$\left.\frac{\partial F(M)}{\partial M}\right|_{M_0} = 2aM_0 + 4bM_0^3 + 6cM_0^5 = 0. \tag{2.18}$$

If we assume that there exist real roots which give a minimum value of the free energy except for $M_0 = 0$, each coefficient must satisfy the relation $a < b^2/3c\,(\equiv a_0)$. Furthermore, if $a < b^2/4c\,(\equiv a_1)$, the free energy of $M_0 \neq 0$ becomes smaller than that of $M_0 = 0$. Therefore, the order parameter in the thermal equilibrium state jumps from $M_0 = 0$ to $M_0 \neq 0$ discontinuously. This corresponds to the first-order phase transition. The free energy with each value of a is plotted in Fig. 2.1.

When $a_1 < a < a_0$, the order parameter in the thermal equilibrium state is $M_0 = 0$. However, the order parameter of $M_0 \neq 0$ also has a local stability near the local minimum. This state is referred to the *metastable state*. Whereas, for $0 < a < a_1$, $M_0 = 0$ becomes metastable. For $a > a_0$ and $a < 0$, metastable states dissappear.

In summary, we show the phase diagram in Fig. 2.2. If $b > 0$, the critical point is located at $a = 0$ and the order parameter becomes finite in $a < 0$. If $b < 0$, however, the metastable state appears at $a = a_0$ and the first-order phase transition occurs at $a = a_1$.

The special point $a = b = 0$ corresponds to the tricritical point for the following reason. If we perform the above analysis with a finite external

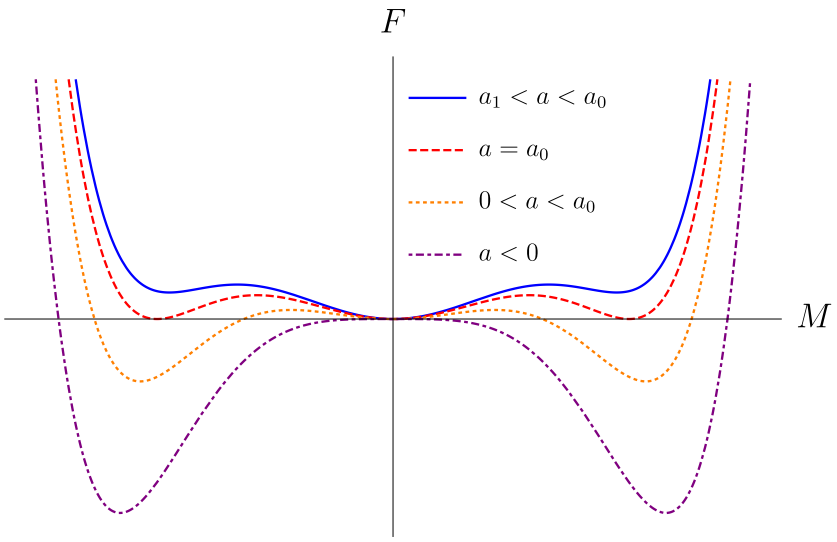

Figure 2.1: The Landau free energy with each value of a as a function of the order parameter M.

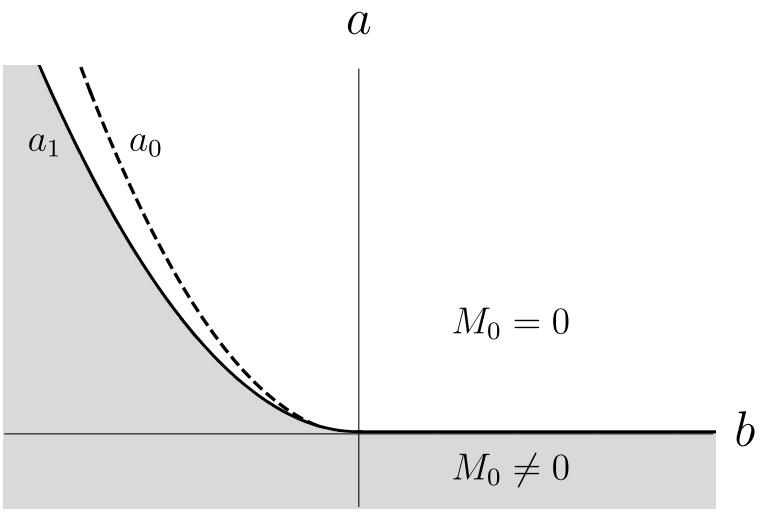

Figure 2.2: The phase diagram with respect to parameters a and b. The gray shaded region indicates the parameter region where the order parameter has finite value $M_0 \neq 0$. The dashed line denotes a_0 at which the metastable state appears. The solid line denotes a_1 at which the first-order phase transition occurs.

field H, we have to add the extra axis of H in the phase diagram. Then, the first-order phase transition line $a = a_1$ forms a plane along both directions of $H > 0$ and $H < 0$. In other words, the phase diagram shown in Fig. 2.2 is considered as a cross-section along the $H = 0$ plane. If we consider a slice with $H \neq 0$, there are the first-order phase transition line and the second-order phase transition point, which is called the critical point. Namely, the second-order phase transition points form a line in the phase diagram with three parameters. The second-order phase transition line exists in each direction of $H > 0$ and $H < 0$ and these lines terminate the origin point. Thus, three coexistence lines terminate at the origin, which is referred to as the *tricritical point*. Fig. 2.3 shows an example of the three-dimensional phase diagram which contains the tricritical point. The tricritical point can also be considered as the point where the second-order phase transition is switched to the first-order phase transition as shown in Fig. 2.2.

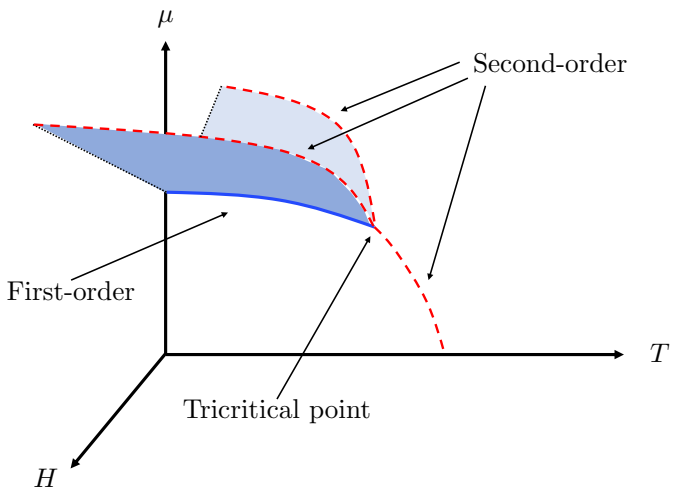

Figure 2.3: The three-dimensional phase diagram which contains the tricritical point. In general, parameters (T, μ, H) depend on what the phase transition we suppose.

Let us compute critical exponents at the tricritical point. Setting $b = H = 0$ in Eq. (2.18), the order parameter is given by

$$M_0 = \left(-\frac{a}{3c}\right)^{1/4} = \left(\frac{k(T_c - T)}{3cT_c}\right)^{1/4}, \tag{2.19}$$

and we obtain $\beta = 1/4$. If we impose an external field, the free energy is rewritten as

$$F(M) = F_0 + aM^2 + bM^4 + cM^6 - HM, \tag{2.20}$$

and the thermal equilibrium is determined by the following equation

$$\left.\frac{\partial F(M)}{\partial M}\right|_{M_0} = 2aM_0 + 4bM_0^3 + 6cM_0^5 - H = 0. \tag{2.21}$$

At the tricritical point, Eq. (2.21) is rewritten by

$$M_0 = \left(\frac{H}{6c}\right)^{1/5}. \tag{2.22}$$

Thus, we obtain $\delta = 5$. The magnetic susceptibility is obtained by differentiating Eq. (2.21) with respect to H. In the vicinity of the tricritical point, the magnetic susceptibility takes the form of

$$\chi = \frac{1}{2a + 30cM_0^4}. \tag{2.23}$$

For $T > T_c$ with $M_0 = 0$, we have

$$\chi = \frac{1}{a} = \frac{T_c}{k(T - T_c)}, \tag{2.24}$$

whereas for $T < T_c$

$$\chi = \frac{1}{2a + 30c(-a/3c)} = -\frac{1}{8a} = \frac{T_c}{8k(T_c - T)}. \tag{2.25}$$

Therefore, we obtain $\gamma = 1$ for both $T > T_c$ and $T < T_c$. Note that the critical amplitude ratio is given by $\chi_{T>T_c}/\chi_{T<T_c} = 8$. The specific heat is obtained by the second derivative of the free energy. For $T < T_c$ with $H = 0$, where the order parameter becomes $M_0^4 = -a/c$, it turns out that the free energy takes the form of $F \propto |T - T_c|^{3/2}$. Thus, we obtain

$$C_v \propto |T - T_c|^{-1/2} \tag{2.26}$$

and we find that $\alpha = 1/2$.

Summarizing the above discussion, we obtain each value of critical exponents at the critical point and the tricritical point in the framework of the Landau theory as shown in Table. 2.1. The Ising model with spin-1 has been known as an example of the model having the tricritical point.

Table 2.1: The values of critical exponents at the critical point and the tricritical point.

critical exponents	critical point	tricritical point
β	1/2	1/4
δ	3	5
γ	1	1
α	0	1/2

2.3 Correlation function

In this section, we take account of the spatial dependence of the order parameter by generalizing the Landau theory shown in Sec. 2.1. We write the order parameter as the function of d-dimensional space coordinates: $M(\boldsymbol{x})$, which describes the average of the magnetization near the position $\boldsymbol{x}$. Then, the correlation function is defined by

$$G(\boldsymbol{x}) = \langle M(\boldsymbol{x})M(0)\rangle \,. \tag{2.27}$$

We begin with the following form of the free energy instead of Eq. (2.1)

$$F = \int d^d x \left(aM(\boldsymbol{x})^2 + b\left(\nabla M(\boldsymbol{x})\right)^2 \right), \tag{2.28}$$

where $a = k(T - T_c)/T_c \equiv kt$ and b is a positive constant. Since the free energy becomes small if the magnetization is spatially homogeneous, the second term describes the ferromagnetic interaction. We can ignore the fourth-order term of the order parameter for the purpose of analyzing the critical phenomena for $T > T_c$. Then, we drop the fourth-order term of the magnetization in the free energy for simplicity. This model is referred to as *the Gaussian model*.

Let us consider the Fourier transformation of the magnetization

$$M(\boldsymbol{x}) = \frac{1}{(2\pi)^d} \int d^d q e^{i\boldsymbol{q}\cdot\boldsymbol{x}} \tilde{M}(\boldsymbol{q}). \tag{2.29}$$

Then, the free energy is rewritten by

$$F = \int \frac{d^d q}{(2\pi)^d} \left(kt + bq^2\right) \tilde{M}(\boldsymbol{q})\tilde{M}(-\boldsymbol{q}). \tag{2.30}$$

The Fourier transform of the correlation function is given by

$$G(\boldsymbol{x}) = \langle M(\boldsymbol{x})M(0)\rangle = \frac{1}{(2\pi)^d}\int d^d q \left\langle \tilde{M}(\boldsymbol{q})\tilde{M}(-\boldsymbol{q})\right\rangle e^{i\boldsymbol{q}\cdot\boldsymbol{x}}, \tag{2.31}$$

where $\tilde{M}(-\boldsymbol{q}) = \tilde{M}(\boldsymbol{q})^*$ is satisfied since $M(\boldsymbol{x})$ must be real. Thus, we would like to compute

$$\tilde{G}(\boldsymbol{q}) \equiv \left\langle \left|\tilde{M}(\boldsymbol{q})\right|^2 \right\rangle \tag{2.32}$$

in order to obtain the correlation function. Since the free energy is given by the quadratic form, we can calculate the expectation value by using the Gaussian integral. The integral variable is $\{\tilde{M}(\boldsymbol{q})\}$ and we have to integrate with respect to both the absolute value $\left|\tilde{M}(\boldsymbol{q})\right| \equiv y_q$ and the phase. Since the free energy does not contain the phase, integration with respect to the phase provides just a constant. If we consider the free energy as the coarse-grained Hamiltonian,

$$\tilde{G}(\boldsymbol{q}) = \frac{\displaystyle\int \prod_{\boldsymbol{q}'} d\tilde{M}(\boldsymbol{q})\left|\tilde{M}(\boldsymbol{q})\right|^2 e^{-\beta F}}{\displaystyle\int \prod_{\boldsymbol{q}'} d\tilde{M}(\boldsymbol{q}) e^{-\beta F}} = \frac{\displaystyle\int dy_q y_q^2 \exp\left(-\beta c_q y_q^2\right)}{\displaystyle\int dy_q \exp\left(-\beta c_q y_q^2\right)}, \tag{2.33}$$

where $c_q = (kt + bq^2)/(2\pi)^2$. Thus, we obtain

$$\tilde{G}(\boldsymbol{q}) = \frac{1}{2\beta c_q} = \frac{(2\pi)^3 T}{2(kt + bq^2)}. \tag{2.34}$$

By performing the inverse Fourier transformation, we obtain the correlation function

$$G(\boldsymbol{x}) = \frac{T}{2}\int d^d q e^{i\boldsymbol{q}\cdot\boldsymbol{x}} \frac{1}{kt + bq^2}. \tag{2.35}$$

Moreover, we can evaluate this integration and the r dependence of the correlation function turns out to be

$$G(\boldsymbol{x}) \propto r^{-(d-1)/2} e^{-r/\xi} \qquad (r \gg 1), \tag{2.36}$$

where ξ is the correlation length given by

$$\xi = \sqrt{\frac{b}{kt}} = \sqrt{\frac{bT_c}{k(T - T_c)}}. \tag{2.37}$$

The relation of Eq. (2.36) is known as *the Ornstein-Zernike formula*. At the critical point $t = 0$, where ξ diverges, we obtain

$$G(\boldsymbol{x}) \propto r^{-d+2}. \tag{2.38}$$

Let us define the critical exponents ν and η by

$$\xi \propto |T - T_c|^{-\nu} \qquad (T > T_c), \tag{2.39}$$

$$G(r) \propto r^{-d+2-\eta} \qquad (T = T_c). \tag{2.40}$$

From Eqs. (2.37) and (2.38), we find that $\nu = 1/2$ and $\eta = 0$.

In the section, we discuss critical exponents in the framework of the Landau theory. These results are reliable if we can ignore the effect of the fluctuations around the mean value of the order parameter. It has been known that these values of the critical exponents are exact for $d > 4$, which is referred to as *the upper critical dimension*. On the other hand, since we cannot ignore the effect of the fluctuations for $d < 4$, the values of critical exponents are different from those of the above discussion in lower dimensional space. Note that the upper critical dimension for the tricritical point is three i.e., the values of critical exponents at the tricritical point shown in Table 2.1 are reliable for $d > 3$.

2.4 Dynamical critical phenomena

In this section, we review the characteristic behavior of the non-equilibrium state near the critical point, so-called *dynamical critical phenomena*. Here, we demonstrate the dynamical critical phenomena by using the Gaussian model. Let us begin with the following equation of motion for a single particle

$$\frac{dp(t)}{dt} = -\Gamma \frac{\partial H}{\partial p} + \zeta(t), \tag{2.41}$$

where $\zeta(t)$ is a random force whose mean is zero and variance is given by

$$\left\langle \zeta(t)\zeta(t') \right\rangle = 2D\delta(t - t') \tag{2.42}$$

with a constant D. If we use Hamiltonian for a free particle, the equation of motion can be written as

$$\frac{dp(t)}{dt} = -\Gamma v(t) + \zeta(t). \tag{2.43}$$

This equation is known as *Langevin equation*, which models the Brownian motion of a single particle. Let us generalize Eq. (2.41) to a system with

multi-degrees of freedom. We assume that the time-dependent order parameter $M(t, \boldsymbol{x})$ is evolved by the following equation

$$\frac{\partial M(t, \boldsymbol{x})}{\partial t} = -\int d^d x' \, \Gamma(\boldsymbol{x} - \boldsymbol{x}') \frac{\delta F}{\delta M(t, \boldsymbol{x}')} + \zeta(t, \boldsymbol{x}), \tag{2.44}$$

where F is a free energy and $\zeta(t, \boldsymbol{x})$ is a random force satisfying

$$\left\langle \zeta(t, \boldsymbol{x}) \zeta(t', \boldsymbol{x}') \right\rangle = 2T\Gamma(\boldsymbol{x} - \boldsymbol{x}')\delta(t - t'). \tag{2.45}$$

The equation (2.44) has been known as *time-dependent Ginzburg-Landau (TDGL) equation*. The TDGL equation has often been used to describe the dynamical behavior of a macroscopic quantity phenomenologically.

The free energy of the Gaussian model is given by Eq. (2.28). Integrating by parts, the free energy is written as

$$F = \int d^d x \left(aM(t, \boldsymbol{x})^2 - bM(t, \boldsymbol{x}) \nabla^2 M(t, \boldsymbol{x}) \right). \tag{2.46}$$

Then, we obtain

$$\frac{\delta F}{\delta M(t, \boldsymbol{x}')} = 2aM(t, \boldsymbol{x}') - b\nabla^2 M(t, \boldsymbol{x}'). \tag{2.47}$$

Substituting (2.47) into (2.44) and performing the Fourier transformation, the TDGL equation is rewritten by

$$\frac{\partial M(t, \boldsymbol{q})}{\partial t} = -(2a + bq^2)\tilde{\Gamma}(\boldsymbol{q})\tilde{M}(t, \boldsymbol{q}) + \tilde{\zeta}(\boldsymbol{q}). \tag{2.48}$$

If we take the average of this equation, we obtain

$$\frac{\partial \left\langle M(t, \boldsymbol{q}) \right\rangle}{\partial t} = -(2a + bq^2)\tilde{\Gamma}(\boldsymbol{q}) \left\langle \tilde{M}(t, \boldsymbol{q}) \right\rangle. \tag{2.49}$$

Thus, we find that the expectation value of the order parameter behaves as

$$\left\langle \tilde{M}(t, \boldsymbol{q}) \right\rangle \propto e^{-t/\tau_q}, \tag{2.50}$$

where τ_q is the relaxation time given by

$$\tau_q = \frac{1}{(2a + bq^2)\tilde{\Gamma}(\boldsymbol{q})}. \tag{2.51}$$

If $\tilde{\Gamma}(\boldsymbol{q})$ becomes finite in the limit of $\boldsymbol{q} \to 0$, the relaxation time in the long wavelength limit becomes

$$\tau_0 = \frac{1}{2a\tilde{\Gamma}(0)} \propto (T - T_c)^{-1}. \tag{2.52}$$

In this case, we find that the relaxation time diverges at the critical point. In other words, since the fluctuations become large near the critical point, the relaxation into the equilibrium state slows down. This phenomenon is called *critical slowing down*. The relaxation time is also written as

$$\tau_0 \propto \xi^z, \tag{2.53}$$

where z is the *dynamical critical exponent*. By using the previous result of $\nu = 1/2$, we find that $z = 2$.

If the total value of the order parameter in the system is a conserved quantity, we find that

$$\frac{\partial \tilde{M}(0,t)}{\partial t} = 0, \tag{2.54}$$

which means that $\tilde{\Gamma}(\boldsymbol{q})$ goes to zero in the limit of $\boldsymbol{q} \to 0$ as can be seen from Eq. (2.49). Moreover, $\tilde{\Gamma}(\boldsymbol{q})$ should be an even function of $\boldsymbol{q}$ because of the inversion symmetry $\Gamma(\boldsymbol{x}) = \Gamma(-\boldsymbol{x})$. Thus, small q expansion would yield $\tilde{\Gamma}(q) = \gamma q^2 + \mathcal{O}(q^4)$. Therefore, the relaxation time is

$$\tau_q = \frac{1}{(2a + bq^2)\gamma q^2} = \frac{\xi^4/\gamma}{c(\xi q)^2 + b(\xi q)^2}, \tag{2.55}$$

where we use $a \propto (T - T_c) \propto \xi^{-2}$ and c is a constant. Provided we consider the spatial region in which ξq is small, we find that τ_q is proportional to ξ^4 and $z = 4$. In Table 3.1, we summarize the dynamical critical exponents in the Gaussian model.

Table 2.2: The values of dynamical critical exponent at the critical point in the Gaussian model

critical exponent	Gaussian model
z	2 (non-conserved)
z	4 (conserved)

As we mentioned in the previous section, we have to note that these results are obtained from the mean-field theory. If we are interested in the

dynamical critical phenomena beyond the mean-field theory, we have to take care of another relaxation mode or the presence of other conserved quantities. The dynamical critical phenomena have been systematically studied by using the renormalization group technique by Hohenberg and Halperin [13].

Chapter 3

Gauge/Gravity duality

In this chapter, we introduce the gauge/gravity duality, which is a fundamental idea for our study. This duality was originally proposed as the correspondence between the gravity theory in the anti-de Sitter (AdS) spacetime and the conformal field theory (CFT) in the Minkowski spacetime [3]. Therefore, this duality is also called the AdS/CFT correspondence. In Sec. 3.1, we briefly review the AdS/CFT correspondence by following the original conjecture in Ref. [3]. In Sec. 3.2, we show the relationship of the partition function between two different theories following Refs. [4, 5]. In Sec. 3.3, we consider the probe brane model, which provides the flavor degree of freedom into the dual gauge theory.

3.1 AdS/CFT correspondence

In this section, we briefly review the AdS/CFT correspondence, which is originally proposed in Ref. [3]. In the superstring theory, in addition to fundamental strings there exist non-perturbative solitonic objects, which are called *D-branes* [14]. The physical meaning of the D-brane can be understood from two different aspects. First, we consider the D-brane as the hyperplane in which open strings can end. In this case, the D-brane plays a role of the Dirichlet boundary condition for open strings. Second, the D-brane can also be regarded as a dynamical object which is a source of closed strings. In the low-energy limit, the D-brane becomes a source of the gravitational field which deforms the spacetime in the supergravity theory.

3.1.1 Effective action of D-branes

Let us start from the first aspect of the D-brane. Hereafter, we refer the $(p+1)$-dimensional D-brane as Dp-brane. We consider the flat (9+1)-dimensional spacetime background. It has been known that the low energy dynamics of a single Dp-brane in the flat (9+1)-dimensional spacetime is given by the *Dirac-Born-Infeld (DBI) action*

$$S_{\rm DBI} = -T_{Dp} \int d^{p+1}\xi \; e^{-\delta\Phi} \sqrt{-\det(\gamma_{ab} + 2\pi\alpha' F_{ab} + B_{ab})}, \tag{3.1}$$

where γ_{ab} is the pull-back of the spacetime metric onto the worldvolume given by

$$\gamma_{ab} = \frac{\partial X^\mu}{\partial \xi^a} \frac{\partial X^\nu}{\partial \xi^b} \eta_{\mu\nu}. \tag{3.2}$$

The other fields $\delta\Phi = \Phi - \langle\Phi\rangle$, F_{ab}, and B_{ab} denote the shift of the dilaton field Φ from the vacuum expectation value $\langle\Phi\rangle$, the $U(1)$ gauge field, and the Kalb-Ramond field, respectively. The overall factor T_{Dp} is the tension of the Dp-brane, which is given by

$$T_{Dp} = \frac{1}{(2\pi)^p g_s \alpha'^{\frac{p+1}{2}}}. \tag{3.3}$$

Also, ξ^a are the worldvolume coordinates on the brane with $a = 0, 1, \cdots p$ and X^μ are the target-space coordinates with $\mu = 0, 1, \cdots 9$.

Here, we consider the case that the vacuum expectation value of dilaton field is constant $e^\Phi = g_s$, $\delta\Phi = 0$, and the Kalb-Ramond field vanishes, for simplicity. It is useful to use the static gauge

$$X^a = \xi^a, \tag{3.4}$$

then the pull-back metric depends only on the transverse fluctuations X^I

$$\gamma_{ab} = \eta_{ab} + \frac{\partial X^I}{\partial \xi^a} \frac{\partial X^J}{\partial \xi^b} \delta_{IJ}, \tag{3.5}$$

where $I, J = p+1, \cdots, 9-p$. If we expand the DBI action in α', we obtain

$$S_{\rm DBI} = -(2\pi\alpha')^2 T_p \int d^{p+1}\xi \left(\frac{1}{4} F_{ab} F^{ab} + \frac{1}{2} \partial_a \phi^I \partial^a \phi^I + \cdots \right), \tag{3.6}$$

where we define scalar fields by $\phi^I = X^I/(2\pi\alpha')$. Other terms denoted by dots are the higher order contributions in α'. Note that we have ignored the constant term in the action.

So far, we have considered the case of a single Dp-brane. Let us generalize the action to the case of the stack of N_c Dp-branes. Since it has been known that coincident N_c branes give rise to a $U(N_c)$ gauge symmetry, the field strength should be given as the $U(N_c)$ gauge covariant form

$$F_{ab} \equiv F^n_{ab} T_n = \partial_a A_b - \partial_b A_a + i[A_a, A_b], \tag{3.7}$$

where T_n is the generator in the fundamental representation in $U(N_c)$. In addition, the scalar field is also transformed in the $U(N_c)$ group, $\phi^I = \phi^{In} T_n$. We have to replace the partial derivatives of the scalar field by the covariant derivatives of that in order to hold the gauge invariance of the action. Thus, we obtain the DBI action to the leading order in α',

$$S_{\rm DBI} = -(2\pi\alpha')^2 T_p \int d^{p+1}\xi \, {\rm Tr} \left(\frac{1}{4} F_{ab} F^{ab} + \frac{1}{2} D_a \phi^I D^a \phi^I - \frac{1}{4} \sum_{I \neq J} \left[\phi^I, \phi^J \right]^2 \right). \tag{3.8}$$

Here, the covariant derivative is given by $D_a \phi^I = \partial_a \phi^I + i\left[A_a, \phi^I\right]$. This action corresponds to the bosonic part of the $\mathcal{N} = 4$ $U(N_c)$ supersymmetric Yang-Mills action, where $\mathcal{N}$ denotes the number of supersymmetry. Since the overall coefficient of this action should correspond to the coupling constant $1/g^2_{\rm YM}$ in order that the DBI action reduces to the supersymmetric Yang-Mills action in the proper limit, we find that

$$g^2_{YM} = \frac{1}{(2\pi\alpha')^2 T_{Dp}} = (2\pi)^{p-2} g_s {\alpha'}^{\frac{p-3}{2}} = (2\pi)^{p-2} g_s l_s^{p-3}, \tag{3.9}$$

where l_s is the length of the string and we have used the relation of $\alpha' = l_s^2$.

3.1.2 D-branes in supergravity

Let us now move to the second aspect of the Dp-brane. A flat Dp-brane has the symmetry $SO(1,p) \times SO(9-p)$. This can be also seen from the low energy effective action of the Dp-brane Eq. (3.8); $SO(1,p)$ is the Lorentz group and $SO(9-p)$ is a global symmetry which rotates the scalar fields ϕ^I. Moreover, if we consider the type IIB superstring theory, there exist 32 supercharges in total. A flat Dp-brane is invariant under half of them, which often referred as *the Bogomolny-Prasad-Sommerfield (BPS) state* [15, 16] . It has been known

that a flat Dp-brane is a BPS solution in type IIB supergravity given by

$$
\begin{aligned}
ds^2 &= H_p(r)^{-1/2}\eta_{\mu\nu}dx^\mu dx^\nu + H_p^{1/2}dx^I dx^I, && (3.10)\\
e^{-\Phi} &= g_s H_p(r)^{(3-p)/4}, && (3.11)\\
C_{(p+1)} &= \left(H_p(r)^{-1}-1\right)dx^0\wedge dx^1\wedge\cdots\wedge dx^p, && (3.12)\\
B_{MN} &= 0, && (3.13)
\end{aligned}
$$

where r is defined by $r^2=\sum_{I=p+1}^{9}x_I^2$. $H_p(r)$ is a harmonic function

$$
H_p(r) = 1+\left(\frac{L}{r}\right)^{7-p}, \tag{3.14}
$$

where L is a characteristic length determined by the charge of the Dp-brane. In the case of N_c coincident Dp-branes, L is given by

$$
L^{7-p} = (4\pi)^{(5-p)/2}\Gamma\left(\frac{7-p}{2}\right)g_s N_c l_s^{7-p}. \tag{3.15}
$$

In supergravity theory, there are also near-extremal non-BPS solutions, the so-called *black p-brane solutions* given by

$$
ds^2 = H_p(r)^{-1/2}\left(-f(r)dt^2+(dx^i)^2\right)+H_p^{1/2}\left(\frac{dr^2}{f(r)}+r^2d\Omega_{8-p}^2\right), \tag{3.16}
$$

$$
f(r) = 1-\left(\frac{r_H}{r}\right)^{7-p}, \tag{3.17}
$$

where r_H is the location of the event horizon. The dilaton and Ramond-Ramond field $C_{(p+1)}$ are the same forms as in the Dp-brane case.

3.1.3 AdS$_5$/CFT$_4$ correspondence

Now we study the type IIB superstring theory with N_c coincident flat D3-branes in the flat (9+1)-dimensional Minkowski spacetime. Here, we consider the open and closed strings as small perturbations, i.e., the coupling constant of strings is sufficiently small; $g_s \ll 1$. Moreover, we have to consider the effective coupling constant g_sN_c for the open strings on the N_c D3-branes.

For $g_sN_c \ll 1$, D3-branes can be considered as the (3+1)-dimensional objects where the open strings can end. In this case, the effective action for all string modes in this theory is written by

$$
S = S_{\text{closed}} + S_{\text{D3}} + S_{\text{int}}, \tag{3.18}
$$

where $S_{\rm closed}$ contains the closed string modes, $S_{\rm D3}$ contains the open string modes, and $S_{\rm int}$ describes the interactions between the closed string modes and the open string modes. If we take the low energy limit of $\alpha' \to 0$, we can ignore the massive string modes. Besides, the open string modes and closed string modes are decoupled since the leading term of $S_{\rm int}$ is the order of α' [1]. In this decoupling limit, the closed string modes become just free supergravity in (9+1)-dimensional Minkowski spacetime and the open string modes are described by the low energy effective action of D3-branes. From Eq. (3.8) the bosonic part of the DBI action in the decoupling limit is written by

$$S_{\rm D3} = -\frac{1}{2\pi g_s}\int d^4\xi\, {\rm Tr}\left(\frac{1}{4}F_{ab}F^{ab} + \frac{1}{2}D_a\phi^I D^a\phi^I - \frac{1}{4}\sum_{I\neq J}\left[\phi^I,\phi^J\right]^2\right). \tag{3.19}$$

Here we use Eq. (3.9) and we find

$$g^2_{\rm YM} = 2\pi g_{\rm s}. \tag{3.20}$$

This relation gives

$$\lambda \equiv g^2_{\rm YM}N_c = 2\pi g_{\rm s}N_c, \tag{3.21}$$

where λ is the 't Hooft coupling. Therefore, we find that the D-brane description is valid only if $\lambda \ll 1$. The action (3.19) corresponds to the bosonic part of the $U(N_c)$ supersymmetric Yang-Mills theory with $\mathcal{N} = 4$, which contains $9-p = 6$ scalar fields ϕ^I and the gauge field A_a. Note that $\mathcal{N} = 4$ supersymmetric Yang-Mills theory is the maximally supersymmetric theory in the four spacetime dimensions, which has the 16 supercharges. These descend from those of the D3-brane which is the BPS state and also has the 16 supercharges. As a result, the N_c coincident D3-branes for $\lambda \ll 1$ are described by the $\mathcal{N} = 4$ $U(N_c)$ supersymmetric Yang-Mills theory in the low energy limit. This theory contains a gauge field, four Weyl fermions, and six real scalar fields.

In the above discussion, we naively take the limit of $\alpha' \to 0$ as the low energy limit. However, we have to fix r/α' in this limit, where r is any distance, for the following reason. Suppose that we add a single D3-brane at $x^9 = r$, while coincident N_c D3-branes are located at $x^9 = 0$. This system is described by a $U(N_c+1)$ gauge theory but reduced to a $U(N_c)\times U(1)$ gauge theory by considering an open string between the D3-brane at $x^9 = r$ and one of D3-branes at $x^9 = 0$. This provides the Higgs

[1]

expectation value $\langle \phi^9 \rangle = r/(2\pi\alpha')$. In the limit of $\alpha' \to 0$, we have to keep this arbitrary energy scale r/α', which corresponds to fixing the massive degrees of freedom. As a result, the precise low energy limit is given by

$$\alpha' \to 0 \quad \text{with} \quad \frac{r}{\alpha'} \text{ fixed.} \tag{3.22}$$

This limit is referred to as the *Maldacena limit*.

For $g_s N_c \gg 1$, the D-brane description is not valid. However, we can consider the D3-branes as the source of the gravitational field as shown in the previous discussion. This description is valid if the curvature of the D3-branes geometry characterized by L is sufficiently small compared to the string scale $l_{\rm s}$. From Eq. (3.15), the characteristic length is given by

$$L^4 = 4\pi g_{\rm s} N_c \alpha'^2. \tag{3.23}$$

Therefore, we require

$$1 \ll \frac{L^4}{\alpha'^2} = 4\pi g_{\rm s} N_{\rm c} = 2\lambda, \tag{3.24}$$

and this is consistent with the fact that the validity of D-brane description ($\lambda \ll 1$) is broken in that region. Thus, we can employ the supergravity solution of $N_{\rm c}$ D3-branes

$$\begin{aligned} ds^2 &= H(r)^{-1/2}(-dt^2 + d\vec{x}^2) + H(r)^{1/2}\left(dr^2 + r^2 d\Omega_5^2\right), && (3.25)\\ e^{\Phi} &= g_{\rm s}, && (3.26)\\ C_{(4)} &= (1 - H(r)^{-1}) dx^0 \wedge dx^1 \wedge \cdots, && (3.27)\\ H(r) &= 1 + \left(\frac{L}{r}\right)^4, && (3.28) \end{aligned}$$

where $\vec{x} = (x^1, x^2, x^3)$ and $d\Omega_5^2$ is the metric on S^5 with unit radius. The radial coordinate is defined by $r^2 = \sum_{I=4}^{9} x_I^2$. Now let us separate the background geometry into two different regions. If $r \gg L$, we can approximate $H(r) \sim 1$. Then, the background metric is reduced to the ten-dimensional flat spacetime. On the other hand, if we focus on the so-called *near horizon region* with $r \ll L$, $H(r)$ is approximated by $H(r) \sim L^4/r^4$ and the metric becomes

$$ds^2 = \frac{r^2}{L^2}\left(-dt^2 + d\vec{x}^2\right) + \frac{L^2}{r^2}\left(dr^2 + r^2 d\Omega_5^2\right). \tag{3.29}$$

This metric (3.29) corresponds to the $\mathrm{AdS}_5 \times S^5$ geometry. Here if we take the low energy limit in this background, the closed string excitations in two

different regions are decoupled from each other. This can be checked as follows. Let us consider the energy $E_{\rm r}$ measured by an observer at a point r and the energy of the string E_∞ measured by an observer at infinitely far from the origin. These are related by the redshift factor

$$E_{\rm r} \sim \frac{d}{d\tau} = \frac{1}{\sqrt{-g_{tt}}}\frac{d}{dt} \sim \frac{1}{\sqrt{-g_{tt}}}E_\infty = H(r)^{1/4}E_\infty. \tag{3.30}$$

In the near horizon region, we obtain

$$E_\infty \sim \frac{r}{L}E_{\rm r} \to 0 \tag{3.31}$$

for $E_{\rm r}$ fixed and $r \ll L$. Thus, we find that the closed string excitation in the near horizon region is measured as the low energy mode by an observer at infinity. This can be understood from the fact that the excitations in the near horizon region become hard to climb the gravitational potential to escape to the asymptotic region. In summary, in the low energy limit, there are two different low energy excitations for an observer at infinity. One is the supergravity modes propagating in flat ten-dimensional spacetime. The other is the excitations in the near horizon region given by the $\mathrm{AdS}_5 \times S^5$ spacetime. These excitations are decoupled from each other due to the low energy limit. Note that in this limit, we have

$$\frac{L^4}{r^4} = 4\pi g_{\rm s} N_{\rm c}\frac{\alpha'^2}{r^4} = 4\pi g_{\rm s} N_{\rm c}\frac{\alpha'^4}{r^4}\frac{1}{\alpha'^2} \to \infty \tag{3.32}$$

with α'/r fixed and $\alpha' \to 0$. Therefore, the Maldacena limit corresponds to taking the limit of $r/L \to 0$ with α'/r fixed, which is referred to as the *near horizon limit*.

To summarize, there are two different perspectives of coincident N_c D3-branes in the flat ten-dimensional Minkowski spacetime. These provide two decoupled effective theories in the low energy limit (see Fig. 3.1).

- For $\lambda \ll 1$, $\mathcal{N} = 4$ $U(N_c)$ supersymmetric Yang-Mills theory on flat (3+1)-dimensional spacetime and type IIB supergravity on flat (9+1)-dimensional spacetime.

- For $\lambda \gg 1$, type IIB supergravity on $\mathrm{AdS}_5 \times S^5$ spacetime and type IIB supergravity on flat (9+1)-dimensional spacetime.

These two perspectives should exhibit the same physics. Since type IIB supergravity on flat (9+1)-dimensional spacetime is identical in both theories,

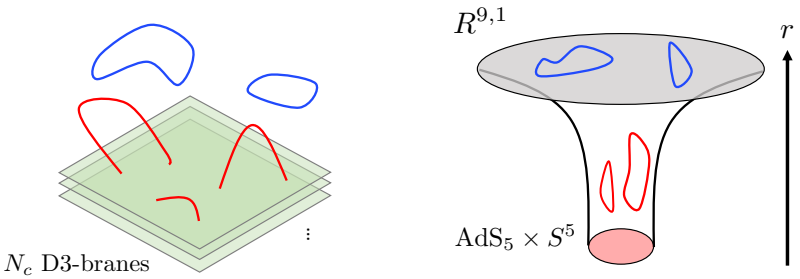

Figure 3.1: Two different perspectives of N_c coincident D3-branes for $\lambda \ll 1$ (left) and $\lambda \gg 1$ (right), respectively.

we are led to the conjecture that $\mathcal{N} = 4$ $U(N_c)$ supersymmetric Yang-Mills theory in flat (3+1)-dimensional spacetime is dual to type IIB supergravity on $\mathrm{AdS}_5 \times S^5$ spacetime.

We have to note that a $U(N_c)$ gauge field is separated into a free $U(1)$ vector multiplet and an $SU(N_c)$ gauge theory. Since all string modes interact with gravity in the dual string theory, the bulk AdS theory is described by the $SU(N_c)$ part of the gauge theory. The $U(1)$ vector multiplet contains six scalar fields, which are related to the center of mass motion of D3-branes. These modes correspond to *singleton* fields in the gravity theory, which are only located at the boundary. Then, we consider the $U(1)$ part decouples from the $SU(N_c)$ part. Therefore, the $\mathrm{AdS}_5/\mathrm{CFT}_4$ correspondence states that $\mathcal{N} = 4$ $SU(N_c)$ *supersymmetric Yang-Mills theory in flat (3+1)-dimensional spacetime is dual to type IIB supergravity on* $AdS_5 \times S^5$ *spacetime* [3].

Let us check the duality from the viewpoint of symmetries. In the $\mathcal{N} = 4$ $SU(N_c)$ supersymmetric Yang-Mills theory, the β function vanishes and this theory is conformal. For example, let us check the β function for 1-loop diagram given by

$$\beta(g_{\mathrm{YM}}) = -\frac{g_{\mathrm{YM}}^3}{48\pi^2} N_c \left(11 - 2n_f - \frac{1}{2}n_s\right), \tag{3.33}$$

where n_f and n_s are the number of Weyl fermions and real scalar fields, respectively. We find $\beta = 0$ because of $n_f = 4$ and $n_s = 6$ in $\mathcal{N} = 4$

supersymmetric Yang-Mills theory. The conformal group in (3+1) dimension is given by $SO(2,4)$. Moreover, the theory has 16 supercharges since it preserves $\mathcal{N}=4$ supersymmetry. The supersymmetry yields the global $SO(6)$ symmetry which corresponds to the rotational transformation of six scalar fields. It can be checked that the $\mathrm{AdS}_5 \times S^5$ geometry has the same symmetry; AdS_5 part has the $SO(2,4)$ symmetry and S^5 part has the $SO(6)$ symmetry. Consequently, the symmetries of these different theories coincide with each other.

3.1.4 Finite temperature

Hitherto we have considered that the dual field theory at zero temperature. However, we can extend it to the finite temperature case by using the near-extremal black 3-brane solution [17] as in Eqs. (3.16) and (3.17) in the gravity theory side. In the near horizon limit, we obtain the metric

$$ds^2 = \left(\frac{r}{L}\right)^2 \left(-f(r)dt^2 + d\vec{x}^2\right) + \left(\frac{L}{r}\right)^2 \left(\frac{dr^2}{f(r)} + r^2 d\Omega_5^2\right), \quad (3.34)$$

$$f(r) = 1 - \left(\frac{r_H}{r}\right)^4, \quad (3.35)$$

where r_H denotes the location of the black hole horizon. This solution is the *Schwarzschild AdS_5 black hole*. In the AdS/CFT correspondence, the thermodynamic quantities of the black hole can be interpreted as those of the strongly coupled dual field theory. For example, the heat bath temperature in the dual gauge field theory is given by the Hawking temperature of the black hole given by $T_H = r_H/(\pi L^2)$.

3.2 GKP-Witten relation

The gauge/gravity duality proposes a map between two different theories as shown in the example of the $\mathrm{AdS}_5/\mathrm{CFT}_4$ correspondence. This map provides a field-operator map between the fields in the gravity theory and operators in the dual gauge field theory. In general, the field-operator map for generating functionals is known as *Gubser-Klebanov-Polyakov (GKP)-Witten relation* [4, 5] which is described by

$$\left\langle \exp\left(\int d^d x \phi^{(0)} \mathcal{O}\right)\right\rangle = e^{-\mathcal{S}\left[\phi_{\mathrm{bdy}}=\phi^{(0)}\right]}. \quad (3.36)$$

Here, the left-hand side of Eq. (3.36) describes the partition function of d-dimensional gauge theory with a source term and the right-hand side of

Eq. (3.36) describes the partition function of (d+1)-dimensional supergravity theory. $\phi^{(0)}$ is a source field and $\mathcal{O}$ is the dual operator in the gauge theory. Note that the strong form of the gauge/gravity duality proposes that the right-hand side of Eq. (3.36) is replaced by $Z_{\rm string}$, which is the superstring partition function. However, in the weak form of the duality, we approximate the superstring partition function by

$$Z_{\rm string} \approx e^{-\mathcal{S}}, \tag{3.37}$$

where $\mathcal{S}$ is the on-shell action in the supergravity theory. This relation enables us to compute the correlation functions in the gauge theory by evaluating the on-shell action in the supergravity theory.

3.2.1 Scalar field

Let us check the relation by considering a couple of examples. We consider the action in the supergravity theory given by

$$\mathcal{S} = \frac{1}{16\pi G_5}\int d^5x\sqrt{-g}(R-2\Lambda) + \mathcal{S}_{\rm matter}, \tag{3.38}$$

where $\mathcal{S}_{\rm matter}$ is the action for matter fields such as scalar fields or vector fields. One of the solutions of the equation of motion from the action (3.38) is the asymptotically AdS_5 spacetime given by

$$ds^2 = \left(\frac{r}{L}\right)^2\left(-dt^2+d\vec{x}^2\right)+\left(\frac{L}{r}\right)^2 dr^2 \qquad (r\to\infty) \tag{3.39}$$

$$= \left(\frac{L}{u}\right)^2\left(-dt^2+d\vec{x}^2+du^2\right) \qquad (u\to 0), \tag{3.40}$$

where $u \equiv L^2/r$. Hereafter, we employ the coordinate system used in Eq. (3.40).

We consider the massless scalar field as the bulk field. The action for matter fields is given by

$$\mathcal{S} = -\frac{1}{2}\int d^5x\sqrt{-g}\,(\nabla\phi)^2\,. \tag{3.41}$$

Here we assume $\phi = \phi(u)$ and $L = 16\pi G_5 = 1$ for simplicity. Since we need the action at AdS boundary $(u \to 0)$, we consider the asymptotic form of

the action[2]

$$\mathcal{S} \sim \int d^4x du \left(-\frac{1}{2u^3}\phi'^2\right) \tag{3.42}$$

$$= \int d^4x \int_0^\infty du \left(\left(-\frac{1}{2u^3}\phi\phi'\right)' + \left(\frac{1}{2u^3}\phi'\right)'\phi\right) \tag{3.43}$$

$$= \int d^4x \frac{1}{2u^3}\phi\phi'\Big|_{u=0} + \int d^4x du \left(\frac{1}{2u^3}\phi'\right)'\phi. \tag{3.44}$$

Here, we used integration by parts in the second line. The second term of (3.44) vanishes for on-shell action since the equation of motion for the scalar field at the AdS is given by

$$\left(\frac{1}{2u^3}\phi'\right)' \sim 0. \tag{3.45}$$

Thus, the asymptotic solution of the scalar field is given by

$$\phi \sim \phi^{(0)}\left(1 + \phi^{(1)}u^4\right), \qquad (u \to 0). \tag{3.46}$$

By using the equation of motion and substituting the asymptotic solution of the scalar field into the action, we obtain the on-shell action

$$\mathcal{S}\left[\phi^{(0)}\right] = 2\int d^4x \left(\phi^{(0)}\right)^2 \phi^{(1)}. \tag{3.47}$$

If we use the GKP-Witten relation, we obtain the 1-point function of the dual operator $\mathcal{O}$

$$\langle\mathcal{O}\rangle = \frac{\delta\mathcal{S}\left[\phi^{(0)}\right]}{\delta\phi^{(0)}} = 4\phi^{(1)}\phi^{(0)}. \tag{3.48}$$

As a result, the asymptotic form of the scalar field is rewritten by

$$\phi \sim \phi^{(0)} + \frac{1}{4}\langle\mathcal{O}\rangle u^4, \qquad (u \to 0). \tag{3.49}$$

In this example, we find that the first term $\phi^{(0)}$ can be considered as the source term and the coefficient of the second term $\langle\mathcal{O}\rangle$ can be considered as the expectation value of the conjugate operator in the asymptotic form of the bulk field.

[2]For simplicity, we discuss near the AdS boundary. However, the result is not changed if we consider all region of the bulk.

In general case of the scalar field in (d+1)-dimensional AdS background spacetime, the action for matter fields is given by

$$\mathcal{S} = -\frac{1}{2}\int d^{d+1}x\sqrt{-g}\left((\nabla\phi)^2 + m^2\phi^2\right), \tag{3.50}$$

where m is the mass of the scalar field. The equation of motion is given by the Klein-Gordon equation

$$\left(\Box - m^2\right)\phi = 0, \tag{3.51}$$

$$\Box\phi = \frac{1}{\sqrt{-g}}\partial_\mu\left(\sqrt{-g}g^{\mu\nu}\partial_\nu\phi\right) \tag{3.52}$$

Eq. (3.52) is explicitly given by

$$\Box\phi = \frac{1}{L^2}\left(u^2\partial_u - (d-1)\,u\partial_u + u^2\eta_{ij}\partial^i\partial^j\right)\phi, \tag{3.53}$$

where $\mu,\nu = 0,1,\cdots,d+1$ and $i,j = 0,1,\cdots,d$. Note that we again use L as the AdS radius to discuss general case. It is convenient to perform a Fourier decomposition in the x^i directions with a plane wave ansatz $\phi(u,x) = e^{ip^ix_i}\phi_p(u)$. Then, the Klein-Gordon equation for the mode $\phi_p(u)$ is written by

$$u^2\phi_p''(u) - (d-1)u\phi_p'(u) - (m^2L^2 + p^2u^2)\phi_p(u) = 0, \tag{3.54}$$

where $p^2 = \eta_{ij}p^ip^j$. The equation of motion provides two different asymptotic solutions

$$\phi_p(u) \sim u^{\Delta_\pm}, \tag{3.55}$$

where $\Delta_\pm$ are given by the roots of $m^2L^2 = \Delta(\Delta - d)$:

$$\Delta_\pm = \frac{d}{2} \pm \sqrt{\frac{d^2}{4} + m^2L^2}. \tag{3.56}$$

Thus, the asymptotic form of the scalar field can be written by

$$\phi(u,x) \sim \phi^{(0)}u^{\Delta_-} + c\,\langle\mathcal{O}\rangle\,u^{\Delta_+}, \qquad (u\to 0) \tag{3.57}$$

where c is a constant. The first term and the second term of Eq. (3.57) are referred to as *non-normalizable mode* and *normalizable mode*, respectively. In general, we can identify the normalizable mode $\langle\mathcal{O}\rangle$ as the vacuum expectation value for a dual operator with conformal dimension Δ_+ and the non-normalizable mode $\phi^{(0)}$ as the source for this operator. Here, this terminology is derived from the finiteness of the action evaluated on the solution.

Let us check this for the action (3.50) for a scalar field $\phi = \phi(u)$. The action is written as

$$\mathcal{S} = -\frac{L^{d-1}}{2}\int d^{d+1}x \frac{1}{u^{d+1}}\left(u^2\phi'^2 + m^2L^2\phi^2\right). \tag{3.58}$$

If we substitute $\phi \sim u^{\Delta}$ into the action and integrate from $u = 0$ to $u = \varepsilon$, we obtain

$$\begin{aligned}\mathcal{S}' &= -\frac{L^{d-1}}{2}\int d^dx \int_0^{\varepsilon} du \left(\Delta^2 + m^2L^2\right) u^{2\Delta-d-1} \\ &= -\frac{L^{d-1}}{2}\int d^dx \frac{\Delta^2 + m^2L^2}{2\Delta - d}u^{2\Delta-d}\Big|_{u=0}^{u=\varepsilon}.\end{aligned} \tag{3.59}$$

Thus, we find that the action is finite for normalizable mode $\Delta = \Delta_+ > d/2$, while diverges for non-normalizable mode $\Delta = \Delta_- < d/2$.

Note that in flat spacetime fields with negative m^2 leads to instability, while in (d+1)-dimensional AdS spacetime scalar fields are still stable even for negative m^2 if the following condition is satisfied:

$$m^2L^2 \geq -\frac{d^2}{4}. \tag{3.60}$$

This lower bound is referred to as *the Breitenlohner-Freedman bound* [18].

3.2.2 Vector field

We consider a vector field as another example of the GKP-Witten relation. We assume that the action for matter fields contains the $U(1)$ gauge field whose action is given by

$$\mathcal{S} = -\frac{1}{4}\int d^5x\sqrt{-g}F^{\mu\nu}F_{\mu\nu}. \tag{3.61}$$

Here we consider the following ansatz for the gauge field

$$A_\mu dx^\mu = A_0(u)dt. \tag{3.62}$$

In a similar way with the previous section, the asymptotic form of the action in the asymptotic AdS spacetime is given by

$$\begin{aligned}\mathcal{S} &\sim \frac{1}{2}\int d^4xdu\frac{1}{u}\left(A_0'\right)^2 \\ &= \frac{1}{2}\int d^4x\int_0^{\infty} du\left(\left(\frac{1}{u}A_0'A_0\right)' - \left(\frac{1}{u}A_0'\right)'A_0\right) \\ &= \int d^4x\,\frac{1}{2u}A_0'A_0\Big|_{u=0} + \int d^4xdu\left(\frac{1}{2u}A_0'\right)'A_0.\end{aligned} \tag{3.63}$$

Here we set L to be unity again. Since the equation of motion is given by

$$\left(\frac{1}{u}A_0'\right)' = 0, \tag{3.64}$$

the asymptotic solution of the gauge field is written as

$$A_0 \sim A_0^{(0)}\left(1 + A_0^{(1)}u^2\right). \qquad (u \to 0) \tag{3.65}$$

The second term of the action (3.63) vanishes by using the equation of motion. Thus, the GKP-Witten relation leads to the expectation value of the dual operator J^0

$$\left\langle J^0 \right\rangle = \frac{\delta \mathcal{S}\left[A_0^{(0)}\right]}{\delta A_0^{(0)}} = 2A_0^{(0)}A_0^{(1)}. \tag{3.66}$$

As a result, we obtain

$$A_0 \sim \mu + \left\langle J^0 \right\rangle u^2, \qquad (u \to 0) \tag{3.67}$$

where $\mu \equiv A_0^{(0)}$, which corresponds to the chemical potential. Similarly, we can obtain the asymptotic form of the gauge field A_x

$$A_x \sim A_x^{(0)} + \langle J^x \rangle u^2, \qquad (u \to 0) \tag{3.68}$$

where the dual operator $\langle J^x \rangle$ is the expectation value of the current density. These relations corresponds to the results obtained from the linear response theory.

3.3 Probe brane model

In this section, we consider the gravity model which is dual to the gauge theory containing flavor degrees of freedom. To realize this system, we consider additional D-branes which are placed in the dual geometry after we have taken the near horizon limit. The additional D-branes modify the original AdS/CFT correspondence and give rise to degrees of freedom that transform as the fundamental representation of the gauge group [19]. This is in contrast to the fields in $\mathcal{N} = 4$ supersymmetric Yang-Mills theory, which transform as the adjoint representation of the gauge group. In general, the additional D-branes change the geometry of D3-branes. However, by taking an appropriate limit, we can treat the additional D-branes as *probes*, which does not affect the D3-brane geometry. This system is referred to as *the probe brane model*.

3.3.1 D3-Dp system

Let us consider a stack of N_c D3-branes and a stack of N_f Dp-branes. In this setup, there are four types of open strings. We have already mentioned the 3-3 strings which end on a stack of D3-branes. The others are the 3-p, p-3, and p-p strings. The 3-p strings end on a stack of D3-branes and a stack of Dp-branes. In the p-3 strings, the beginning point and the ending point are interchanged in contrast to the 3-p strings. The p-p strings end on a stack of Dp-branes.

Let us compare the 't Hooft coupling of the gauge theory on the Dp-branes to that on the D3-branes. For the D3-branes, we have already seen

$$\lambda_{D3} \equiv 2\pi g_{\rm s} N_c. \tag{3.69}$$

On the other hand, for the Dp-branes we have

$$\lambda_{{\rm D}p} \equiv (2\pi)^{p-2} \alpha'^{(p-3)/2} g_{\rm s} N_f. \tag{3.70}$$

As a result, we obtain

$$\frac{\lambda_{Dp}}{\lambda_{D3}} = \frac{N_f}{N_c} (2\pi)^{p-3} \alpha'^{(p-3)/2}. \tag{3.71}$$

For $p > 3$, since the quotient vanishes in the Maldacena limit $\alpha' \to 0$, the p-p strings are non-dynamical. For $p < 3$, it diverges in the Maldacena limit i.e. we have to consider the gauge bosons which arise from p-p strings.

To consider the stable D3-Dp system, we require that the D3-Dp intersection is supersymmetric. This condition is satisfied by requiring the number of Neumann-Dirichlet directions is 0, 4, or 8. Moreover, the Dp-branes must extend the time-direction and at least one direction perpendicular to the D3-branes. These conditions restrict the possible Dp-brane embeddings in a stack of D3-branes.

3.3.2 D3-D7 model

An important example of probe brane models is the D3-D7 model, which has widespread applications in the AdS/CFT correspondence. Let us see the D-brane perspective in this system. It has been known that the dual field theory of the D3-D7 model is (3+1) dimensional $\mathcal{N} = 4$ Super Yang-Mills theory coupled to flavor fields preserving $\mathcal{N} = 2$ supersymmetry. In the D3-D7 model, the N_c D3-branes and the N_f D7-branes are extended along each direction as shown in Table. 3.1. We denote ✓ as directions which are

Table 3.1: Embedding directions of the D3-branes and the D7-branes

	0	1	2	3	4	5	6	7	8	9
D3	✓	✓	✓	✓	-	-	-	-	-	-
D7	✓	✓	✓	✓	✓	✓	✓	✓	-	-

filled by the D3-branes and the D7-branes and − as directions perpendicular to these branes.

After the Maldacena limit has been taken, the 7-7 strings decoupled from the 3-3, 3-7, and 7-3 strings. The 3-3 strings gives rise to the degrees of freedom of $\mathcal{N} = 4$ supersymmetric Yang-Mills theory as we explained in the previous section. On the other hand, the 3-7 and 7-3 strings correspond to excitations in the $\mathbf{N}$ and $\bar{\mathbf{N}}$ of $SU(N_c)$, respectively. Thus, these excitations transform in the fundamental and anti-fundamental representation of the $SU(N_c)$ gauge theory.

Symmetries in the gravity description of the D3-D7 model correspond to those in the dual field theory. First, the local gauge symmetry of $U(N_f)$ in the D3-D7 model is mapped to the global $U(N_f)$ flavor symmetry in the dual field theory. The $U(1)_B$ symmetry is a subgroup of the $U(N_f)$ flavor group. This global $U(1)_B$ symmetry provides the baryon charge in the dual field theory Moreover, the D3-D7 model has an $SO(4) \times SO(2)$ isometry in the directions perpendicular to the D3-branes. The $SO(4)$ group rotates the 4567 directions which is filled by the D7-branes and the $SO(2)$ group rotates the 89 directions which is perpendicular to the D7-branes. The $SO(4)$ rotational symmetry can be decomposed into two $SU(2)$ groups, denoted by $SU(2)_L$ and $SU(2)_R$. The $SU(2)_R$ symmetry is mapped to the $\mathcal{N} = 2$ R-symmetry $SU(2)_R$ on the field theory side. On the other hand, the $SU(2)_L$ symmetry is identified with $SU(2)_\Phi$, which rotates two complex scalars in the adjoint hypermultiplet.

If we separate the D7-branes from the D3-branes in the 89 directions, the $SO(2)$ rotational symmetry is explicitly broken. For example, by placing the D7-branes at $x^8 = l_q$ and $x^9 = 0$, this provides the quark mass in the dual gauge field theory given by

$$m_q = \frac{l_q}{2\pi\alpha'}. \tag{3.72}$$

In other words, if we consider the massive quark in the dual gauge field theory, $SO(2)$ rotational symmetry in the gravity theory side, which corresponds to the $U(1)_R$ chiral symmetry in the dual gauge field theory side, is

broken.

On the supergravity side, the action of the D3-D7 model is described by

$$S = S_{\rm IIB} + S_{D7}, \tag{3.73}$$

where $\mathcal{S}_{\rm IIB}$ shows the D3-branes part in type IIB supergravity theory and $\mathcal{S}_{\rm D7}$ is the DBI action of the D7-branes. In general, we have to consider the *backreaction* from the D7-branes, which give rise to the source terms in the equation of motion of type IIB supergravity.

To analyze the D3-D7 model on the gravity theory side, we take the *probe limit*, i.e. $N_f/N_c \to 0$ in the near horizon limit. In other words, we consider the small number of D7-branes and treat them as the *probe branes*. In this limit, we can neglect the backreaction from the D7-branes on the near horizon geometry to the D3-branes.

Let us consider a single probe D7-brane in $\mathrm{AdS}_5 \times S^5$ which is obtained from the near horizon limit of the D3-branes. The low energy effective dynamics of the probe D7-brane is described by the DBI action

$$S_{D7} = -\frac{T_{D7}}{g_{\rm s}} \int d^8\xi \sqrt{-\det\left(g_{ab} + 2\pi\alpha' F_{ab}\right)}, \tag{3.74}$$

where T_{D7} is the D7-brane tension given by Eq. (3.3). g_{ab} and F_{ab} are the pullback of a bulk field to the worldvolume of the brane and the field strength associated with a $U(1)$ gauge field on the D7-brane, respectively. We write the metric of $\mathrm{AdS}_5 \times S^5$ spacetime in the following form

$$ds^2 = \frac{r^2}{L^2}\left(-dt^2 + d\vec{x}^2\right) + \frac{L^2}{r^2}\left(d\rho^2 + \rho^2 d\Omega_3^2 + dw_5^2 + dw_6^2\right), \tag{3.75}$$

where we write the six coordinates perpendicular to the D3-branes as $w_1, \cdots w_6$. Then we define $\rho^2 = w_1^2 + \cdots w_4^2$ and $r^2 = \rho^2 + w_5^2 + w_6^2$. In addition, we use the static gauge in which the D-brane worldvolume coordinates ξ^a are identified with the spacetime coordinates $x_0, \cdots, x_3$ and $w_1, \cdots, w_4$. The induced metric obtained from the pullback of the metric to the worldvolume of the D7-brane is

$$ds^2_{D7} = \frac{\rho^2 + w_5^2 + w_6^2}{L^2}\left(-dt^2 + d\vec{x}^2\right) + \frac{L^2}{\rho^2 + w_5^2 + w_6^2} d\rho^2 + \frac{L^2\rho^2}{\rho^2 + w_5^2 + w_6^2} d\Omega_3^2. \tag{3.76}$$

Here, we assume that $w_5 = w_5(\rho)$ and $w_6 = 0$ by using the symmetry in the w_5 and w_6 plane. The AdS boundary is located at $\rho \to \infty$. For simplicity,

we set the $U(1)$ gauge field to be zero. In this setup, the DBI action is written as

$$S_{D7} = -\frac{T_{D7}}{g_{\rm s}}\mathrm{Vol}(\mathbb{R}^{1,3})\mathrm{Vol}(S^3)\int d\rho\rho^3\sqrt{1+\dot{w_5}^2}, \tag{3.77}$$

where $\dot{w_5} = dw_5/d\rho$. The configuration of the D7-brane corresponds to the solution of the equation of motion

$$\frac{d}{d\rho}\left(\frac{\rho^3}{\sqrt{1+\dot{w_5}^2}}\dot{w_5}\right) = 0. \tag{3.78}$$

If we consider the asymptotic form of the solution of (3.78), we obtain

$$w_5 = m_q + \frac{c}{\rho^2} + \cdots, \tag{3.79}$$

where m_q and c correspond to the quark mass and the chiral condensate in the dual field theory.

3.3.3 Other models

So far, we focus on the D3-D7 model. However, there are several other probe brane models, for example the D3-D5 model. In the D3-D5 model, the D5-brane is embedded as shown in Table. 3.2. We find that this model also satisfies the conditions of intersections, i.e. there are four Neumann-Dirichlet directions. The crucial difference is that this model has a co-

Table 3.2: Embedding directions of the D3-branes and the D5-branes

	0	1	2	3	4	5	6	7	8	9
D3	✓	✓	✓	✓	-	-	-	-	-	-
D5	✓	✓	✓	-	✓	✓	✓	-	-	-

dimension one intersection: there is one dimension in which the D3-brane extend, but not the D5-brane. This implies that the fundamental flavor fields live in the (2+1)-dimensional spacetime. As a result, the associated field theory becomes a *defect field theory* where (2+1)-matter fields defects couple to a (3+1)-dimensional gauge theory [20].

In the D3-D5 model, the brane intersection preserves 8 supercharges. Hence the dual field theory is $\mathcal{N} = 4$ supersymmetric Yang-Mills theory

in (3+1)-dimensional spacetime coupled to flavor fields preserving (2+1)-dimensional $\mathcal{N} = 4$ supersymmetry. Then, the (3+1)-dimensional $\mathcal{N} = 4$ vector multiplet is decomposed into the (2+1)-dimensional $\mathcal{N} = 4$ vector multiplet and the (2+1)-dimensional hypermultiplet. The bosonic contents of the vector multiplet in the vector field A_k and the three scalars $X_V = (X^7, X^8, X^9)$. The bosonic contents of the hypermultiplet are the scalar field A_3 and the three scalars $X_H = (X^4, X^5, X^6)$. The flavor fields form a (2+1)-dimensional hypermultiplet, which contains two fermions and two complex scalars. For massless flavor fields, the D3-D5 model preserves $SO(2, 3)$ conformal symmetry. On the other hand, the $SO(6)$ R-symmetry is broken down to a subgroup $SU(2)_H \times SU(2)_V$, which corresponds to the symmetries of X_H and X_V, respectively.

Chapter 4

Non-equilibrium phase transition

In this chapter, we show that the non-equilibrium phase transition appears in the NESS regime analyzed by the D3-D7 model. In Sec. 4.1, we study the non-equilibrium phase transitions and critical phenomena in the presence of the current density J and the external electric field E. This non-equilibrium phase transition is associated with the non-linear J-E relation. We find that our non-equilibrium phase transition is both the first-order and the second-order depending on parameters. We analyze critical phenomena of it, focusing on critical exponents. In Sec. 4.2, we study another non-equilibrium phase transition in the same model. Particularly, we find that this phase transition is associated with the $U(1)$ chiral symmetry breaking. Moreover, we discover the novel tricritical point which is realized only in the NESS regime.

4.1 D3-D7 setup for model of conductor

4.1.1 Introduction

In non-equilibrium steady states, the typical additional parameter that is absent in equilibrium systems is *current*. For example, a system attached to two heat baths of different temperatures has a heat current. In this case, the heat current is the "new" parameter, which is special to non-equilibrium systems. Another example is an electric current along an electric field in a conductor. In this case, the equilibrium state is realized in the limiting case that the current vaniseh es.

These new parameters, for example, the heat current and the electric current, measure the rate of entropy production (when the electric field or the temperatures of two heat baths are kept fixed), hence they represent the "distance" from the equilibrium states. A primary question in non-equilibrium physics is how these parameters control the systems. In particular, investigation of phase transitions under the presence of current is one important research subject.[1]

In this section, we study non-equilibrium critical phenomena driven by an electric current density J. When a system exhibits a second-order phase transition under the presence of J, a natural question is how the new parameter J affects the critical phenomena. More specifically, the following questions can be addressed. 1) Is it possible to define a susceptibility with respect to J in a proper way? 2) If yes, how does it behave near the critical point? Are there any critical phenomena associated with the new parameter J? If it is the case, what are the critical exponents? 3) Do we have more critical exponents for non-equilibrium phase transitions than what we have for equilibrium systems? Can we construct a theory for these critical exponents? We try to answer these questions by using the gauge/gravity duality.

4.1.2 Setup

In this section, we realize a conducting system in the D3-D7 model [21]. In the D3-D7 model, the dual field theory contains the gauge particles in the adjoint representation (gluon sector) and the charged particles (quark sector) in the fundamental and anti-fundamental representation. Here the charge is that of the global $U(1)_B$ symmetry, and not that of the color. In this sense, the gluon sector is neutral. We apply a constant external electric field acting on this charge. We take the large-N_c limit to analyze a NESS. The NESS is realized in the limit since the degree of freedom of the gluon sector, which is $\mathcal{O}(N_c^2)$, becomes sufficiently larger than that of the quark sector, which is $\mathcal{O}(N_c)$. Then we can ignore the backreaction to the gluon sector from the quark sector in this limit. As a result, the gluon sector acts as a heat bath for the quark sector. This situation is considered as a NESS with a constant current of the charge. The gravity dual of this situation is described by the D3-D7 setup [19]. The D7-brane is embedded in the background geometry which is a direct product of a 5-dimensional AdS-Schwarzschild black hole (AdS-BH) and S^5. The gluon sector and the

[1] A first-order phase transition in the presence of *heat current* has been studied in [22].

quark sector correspond to AdS-BH and the D7-brane, respectively.

The metric of the AdS-BH part is given by

$$ds^2 = -\frac{1}{z^2}\frac{(1-z^4/z_H^4)^2}{1+z^4/z_H^4}dt^2 + \frac{1+z^4/z_H^4}{z^2}d\vec{x}^2 + \frac{dz^2}{z^2}, \tag{4.1}$$

where z ($0 \leq z \leq z_H$) is the radial coordinate of the geometry. For convenience, we use the Fefferman-Graham coordinate. The boundary is located at $z = 0$, whereas the horizon is located at $z = z_H$. The Hawking temperature is given by $T = \sqrt{2}/(\pi z_H)$. t and $\vec{x}$ denote the (3+1)-dimensional spacetime coordinates of the gauge theory. The metric of the S^5 part is given by

$$d\Omega_5^2 = d\theta^2 + \sin^2\theta d\psi^2 + \cos^2\theta d\Omega_3^2, \tag{4.2}$$

where $0 \leq \theta \leq \pi/2$ and $d\Omega_d$ is the volume element of a d-dimensional unit sphere. For simplicity, the radius of the S^5 part is taken to be 1. This is equivalent to set the 't Hooft coupling λ of the gauge theory at $\lambda = (2\pi)^2/2$.

In our setup, the D7-brane is wrapped on the S^3 part of the S^5. Since the radius of the S^3 part is $\cos\theta$, the configuration of the D7-brane is determined by the function $\theta(z)$. The asymptotic form of $\theta(z)$ is found to be

$$\theta(z) = m_q z + \frac{1}{2}\left(\frac{\langle\bar{q}q\rangle}{N} + \frac{m_q^3}{3}\right)z^3 + \mathcal{O}(z^5), \tag{4.3}$$

where $\langle\bar{q}q\rangle$ denotes the chiral condensate and m_q is the current quark mass [23, 24]. (See also Ref. [21].) Here, we define $N = T_{D7}(2\pi^2) = N_c/(2\pi)^2$ in our convention.

The D7-brane action is given by the Dirac-Born-Infeld (DBI) action:

$$S_{D7} = -T_{D7}\int d^8\xi\sqrt{-\det(g_{ab} + (2\pi\alpha')F_{ab})}. \tag{4.4}$$

Here T_{D7} is the D7-brane tension, ξ are the worldvolume coordinates, g_{ab} is the induced metric and F_{ab} is the $U(1)$ field strength on the D7-brane. The Wess-Zumino term does not contribute in our setup. Assuming the external electric field E is applied along the x direction, the asymptotic form of the gauge field A_x on the D7-brane is related to E as

$$A_x(z,t) = -Et + \text{const.} + \frac{J}{2N}z^2 + \mathcal{O}(z^4). \tag{4.5}$$

Here we have employed the gauge $\partial_z A_t = 0$, which corresponds to the condition that the system has no charge carriers. Thus, the Lagrangian density

in the D7-brane action (4.4) is explicitly written as

$$\mathcal{L}_{D7} = -N\cos^3\theta g_{xx}\sqrt{|g_{tt}|g_{xx}g_{zz} - g_{zz}(\dot{A}_x)^2 + |g_{tt}|(A'_x)^2}, \tag{4.6}$$

where the prime and the dot stand for the differentiation with respect to z and t, respectively. The induced metric agrees with the metric of AdS-BH (4.1) except for $g_{zz} = 1/z^2 + \theta'(z)^2$. According to the AdS/CFT dictionary, the current density J (in the x direction) is given by $J = \partial\mathcal{L}_{D7}/\partial A'_x$ [25].

To make J to be a control parameter, let us perform a Legendre transformation

$$\begin{aligned}\tilde{\mathcal{L}}_{D7} &= \mathcal{L}_{D7} - A'_x\frac{\partial\mathcal{L}_{D7}}{\partial A'_x} \\ &= -\sqrt{\frac{g_{zz}}{|g_{tt}|g_{xx}}}\sqrt{\xi\chi},\end{aligned} \tag{4.7}$$

where

$$\xi = N^2|g_{tt}|g_{xx}^2\cos^6\theta - J^2, \tag{4.8}$$

$$\chi = g_{tt}g_{xx}^2 - g_{xx}E^2. \tag{4.9}$$

The Euler-Lagrange equation for θ yields

$$\frac{\partial}{\partial z}\frac{\partial\tilde{\mathcal{L}}_{D7}}{\partial\theta'} - \frac{\partial\tilde{\mathcal{L}}_{D7}}{\partial\theta} = 0. \tag{4.10}$$

In addition, requiring the on-shell D7-brane action (4.7) to be real, the functions ξ and χ in the square-root must change the sign at the same location on the z-axis, say $z = z_*$, simultaneously. Thus, (i) $\xi = 0$ and (ii) $\chi = 0$ are satisfied at $z = z_*$, which we refer *effective horizon*. The condition (ii) gives us the location of the effective horizon explicitly,

$$z_* = (\sqrt{e^2+1} - e)^{1/2}z_H, \tag{4.11}$$

where e is defined as dimensionless quantity: $e = 2E/(\pi\sqrt{2\lambda}T^2)$. The condition (i) provides the explicit form of the current density

$$J = \pi NT(e^2+1)^{1/4}\cos^3\theta(z_*)E. \tag{4.12}$$

4.1.3 Nonlinear conductivity and non-equilibrium phase transitions

We need to solve the equation of motion (EOM) (4.10) to obtain the relation between J and E. We specify two boundary conditions:

$$\theta(z)/z|_{z=0} = m_q, \tag{4.13}$$

$$\theta'|_{z=z_*} = [C - \sqrt{C^2 + D^2}]/(Dz_*). \tag{4.14}$$

Here $C = 3z_H^8 + 2z_H^4 z_*^4 + 3z_*^8$ and $D = 3(z_*^8 - z_H^8)\tan\theta(z_*)$. The second boundary condition is derived from the EOM at $z = z_*$ [26]. (See also Ref. [27].) Now the problem is reduced to be simple: EOM (4.10), which is the second order non-linear differential equation, and two boundary conditions (4.13) and (4.14).

We have shown that the extremely complicated problem in the field theory side can be reduced to be the simple problem. However, it is generally difficult to solve analytically. Thus, we employ the numerical method. To solve the EOM numerically, we employ the shooting method by using the Mathematica's NDSolve command. Since the numerical analysis becomes unstable at $z = 0$, $z = z_H$ and $z = z_*$, we avoid these points by introducing cutoffs and check the cutoff independence. For simplicity, we set $N = 1$. For technical reasons, after we impose $\theta(z_*) = \theta_0$ for $0 \leq \theta_0 \leq \pi/2$ instead of the first boundary condition of (4.13) and solve the EOM for each θ_0, we pick out solutions so that m_q agrees with the designated value. In Fig. 4.1, we show the mass m_q as a function of the current density J, which are computed from Eq. (4.3) and Eq. (4.12), respectively. We choose $m_q = 1$ for simplicity. As can be seen from Fig. 4.1, there can be two solutions having different values of J for each E. In other words, it shows that there are two possible solutions for given E and m_q. We show the J-E characteristics at several temperatures in Fig. 4.2. Note that since we consider the current density J as the control parameter, we choose the horizontal axis for J. The J-E characteristics show that there are two kinds of regions in our conductor system, namely the negative differential conductivity (NDC) region and the positive differential conductivity (PDC) region.

For $T < T_c$ the NDC region, where the slope of the J-E curve is negative, is smoothly connected to the PDC region, where the slope is positive. On the other hand, for $T > T_c$ there is an intermediate region between the NDC region and the PDC region, where E has three different possible values at a given J. Since we assume that the value of E has to be selected to one of them, E must jump to another value at some point in this region. It was proposed that the transition point is determined by a thermodynamic potential

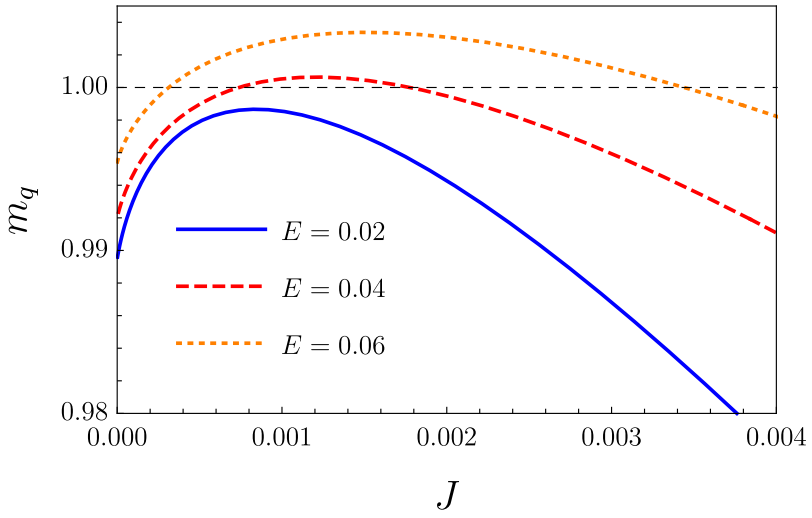

Figure 4.1: The quark mass m_q as a function of the current density J for several E at $T = 0.34285$.

defined by using the Hamiltonian of the D7-brane [28][2]. The Hamiltonian density is given by

$$\begin{aligned}\tilde{\mathcal{H}}_{D7} &= \dot{A}_x \frac{\partial \tilde{\mathcal{L}}_{D7}}{\partial \dot{A}_x} - \tilde{\mathcal{L}}_{D7} \\ &= g_{xx}\sqrt{|g_{tt}|g_{zz}}\sqrt{\frac{N^2\cos^6\theta |g_{tt}| g_{xx}^2 - J^2}{|g_{tt}|g_{xx} - E^2}}. \end{aligned} \tag{4.15}$$

Then the thermodynamic potential is defined as

$$\tilde{F}_{D7}(T, J; m_q) = \lim_{\epsilon \to 0}\left[\int_\epsilon^{z_H} dz \tilde{\mathcal{H}}_{D7} - L_{\text{count}}(\epsilon)\right], \tag{4.16}$$

where L_{count} denotes the counterterms that regularize the divergence at the boundary $z = 0$. L_{count} is given by

$$L_{\text{count}} = L_1 + L_2 - L_F + L_f, \tag{4.17}$$

[2]See also [29], for similar proposal.

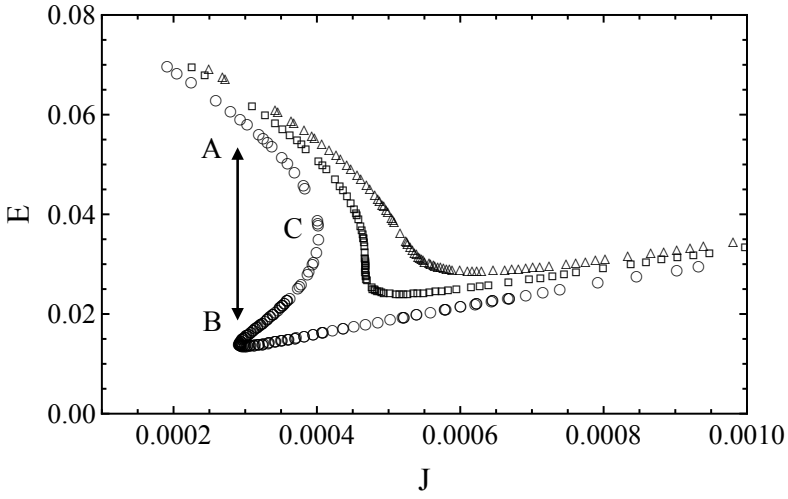

Figure 4.2: The J-E characteristics at various temperatures: $T = 0.34378 > T_c$ (circle), $T = 0.34365 = T_c$ (box), and $T = 0.34356 < T_c$ (triangle).

where each term of (4.17) is given in Ref. [21] as

$$L_1 = \frac{1}{4}\sqrt{-\det\{\gamma_{ij}\}}, \tag{4.18}$$

$$L_2 = -\frac{1}{2}\sqrt{-\det\{\gamma_{ij}\}}\theta(\epsilon)^2, \tag{4.19}$$

$$L_f = \frac{5}{12}\sqrt{-\det\{\gamma_{ij}\}}\theta(\epsilon)^4, \tag{4.20}$$

$$L_F = \frac{1}{2}E^2 \log \kappa\epsilon. \tag{4.21}$$

Here γ_{ij} is the induced metric on the $z = \epsilon$ slice and κ is a factor in order to make the argument of the logarithm dimensionless. The value of κ is scheme dependent, and we have chosen this value as one of the possible choices so that $\partial^2\mathcal{L}_{D7}/\partial E^2 = 0$ for vacuum ($T = 0$, $E = 0$, $m_q \neq 0$). This condition shows that the polarizability vanishes in vacuum. It is natural to require the stable state to have the lowest E at a given J [28]. As a result, the transition point between the NDC phase and the PDC phase is the point indicated by the arrow between A and B in Fig. 4.2. Thus, if we control the current density, the system exhibits the phase transition. In this sense, we consider this phase transition as the *non-equilibrium phase transition*. We call the transition for $T > T_c$ the first-order transition because E changes

discontinuously. We call the transition for $T = T_c$ the second-order transition because the differential resistivity $\partial E/\partial J$ diverges there while $\sigma = J/E$ changes continuously [28].

4.1.4 Critical phenomena

In this subsection, we consider the critical behavior of the non-equilibrium phase transition given in the previous section.

Evaluation of β and δ

In our nonequilibrium phase transition, the critical exponents β and δ are defined in Ref. [28] as

$$\Delta\sigma \propto |T - T_c|^{\beta}, \quad |\sigma - \sigma_c| \propto |J - J_c|^{1/\delta}, \tag{4.22}$$

where T is the heat-bath temperature and $\Delta\sigma$ is the difference of the conductivity between the PDC phase and the NDC phase at a transition point. σ_c and J_c are the conductivity and the current density at the critical point, respectively. $\Delta\sigma$ is evaluated along the line of the first-order phase transition. The value of δ is evaluated along the line of $T = T_c$. These definitions correspond to Eqs. (2.11) and (2.12) in the Landau theory: the definitions (4.22) were proposed by using an assumption that $\sigma - \sigma_c$ and $J - J_c$ play a role of the order parameter and that of the external field, respectively. Our numerical data are shown in Fig. 4.3. We obtain $\beta = 0.505 \pm 0.008$ and $\delta = 3.008 \pm 0.032$.

It has been proposed in Ref. [28] that the chiral condensate $\langle\bar{q}q\rangle$ is another candidate for the order parameter. Then we have another definition of the critical exponents:

$$\Delta \langle\bar{q}q\rangle \propto |T - T_c|^{\beta_{\rm chiral}}, \quad |\langle\bar{q}q\rangle - \langle\bar{q}q\rangle_c| \propto |J - J_c|^{1/\delta_{\rm chiral}}, \tag{4.23}$$

where $\langle\bar{q}q\rangle_c$ is $\langle\bar{q}q\rangle$ at the critical point. We show the numerical results for chiral condensate in Fig. 4.4. We find that these critical exponents are $\beta_{\rm chiral} = 0.515 \pm 0.029$ and $\delta_{\rm chiral} = 2.999 \pm 0.061$. We have reconfirmed the results found in Ref. [28]. Note that all of these values agree with those of the Landau theory, $\beta = 1/2$ and $\delta = 3$, given in (2.16) within the numerical error.

Evaluation of γ

This is the main part of this section which is about the definition and calculation of the critical exponent γ. First, we define the critical exponent γ for

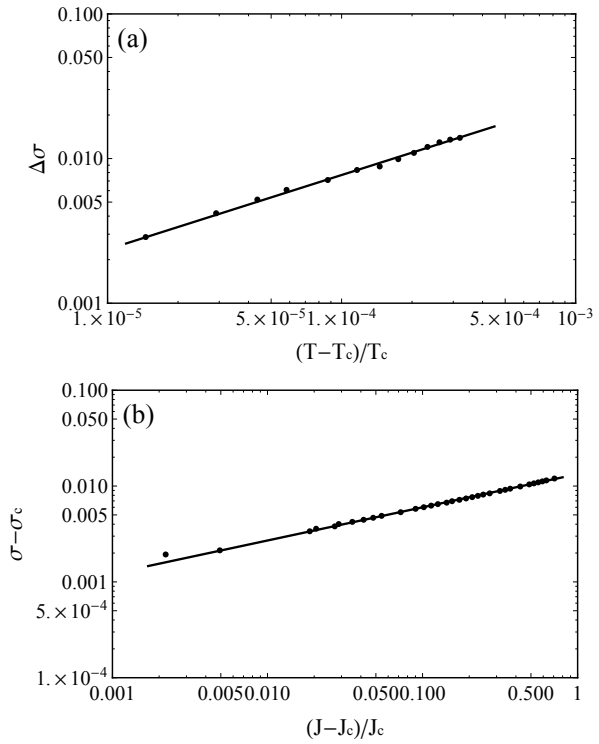

Figure 4.3: (a) Critical behavior of the difference of the conductivity $\Delta\sigma$ near the critical point and (b) that of $\sigma - \sigma_c$.

our non-equilibrium phase transition. In Sec. 2.1, we have reviewed that the critical exponent γ in the Landau theory is defined by using the magnetic susceptibility $\chi = \partial M/\partial H$, where M is the magnetization and H is the external magnetic field. Near the critical point, the magnetic susceptibility behaves as $\chi \propto |T - T_c|^{-\gamma}$. In our non-equilibrium phase transition, since we use either the conductivity or the chiral condensate as the order parameter, it is natural to generalize the definition of χ as

$$\tilde{\chi} = \frac{\partial(\sigma - \sigma_c)}{\partial J}, \quad \tilde{\chi}_{\rm chiral} = \frac{\partial(\langle\bar{q}q\rangle - \langle\bar{q}q\rangle_c)}{\partial J}, \tag{4.24}$$

where J is again assumed to act as the external field. We can rewrite $\tilde{\chi}$ by using the definition of conductivity $\sigma = J/E$,

$$\tilde{\chi} = \frac{1}{E} - \frac{J}{E^2}\frac{\partial E}{\partial J}, \tag{4.25}$$

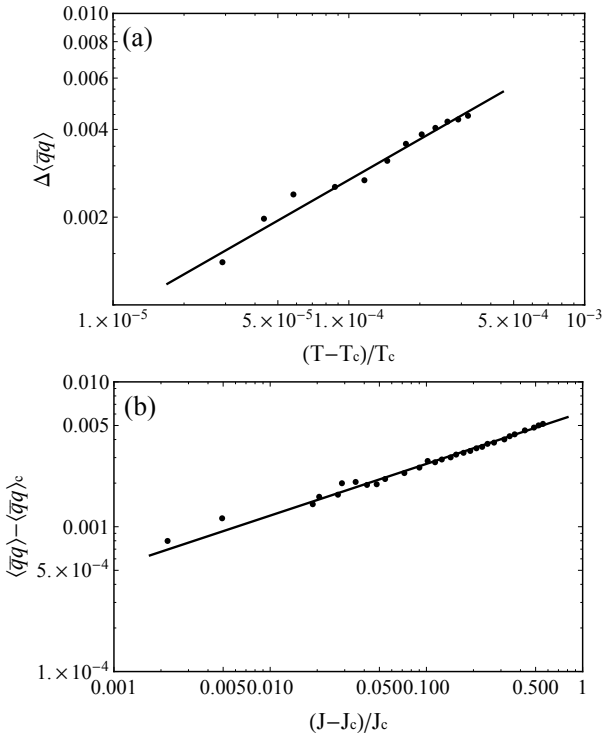

Figure 4.4: (a) Critical behavior of the difference of the chiral condensate $\langle\bar{q}q\rangle$ near the critical point and (b) that of $\langle\bar{q}q\rangle - \langle\bar{q}q\rangle_c$.

so that it can be calculated from the J-E characteristics.

We propose to define the critical exponent γ as

$$\tilde{\chi} \propto |T - T_c|^{-\gamma} \tag{4.26}$$

in our non-equilibrium phase transition.[3] There are two possible definitions of $\tilde{\chi}$ for $T > T_c$ in the NDC phase and in the PDC phase

$$\tilde{\chi}_{\rm NDC} = \frac{\partial(\sigma_{\rm NDC} - \sigma_c)}{\partial J}, \quad \tilde{\chi}_{\rm PDC} = \frac{\partial(\sigma_{\rm PDC} - \sigma_c)}{\partial J}. \tag{4.27}$$

As shown in Fig. 4.5, the behaviors of the susceptibilities in these phases are similar to each other and it is found that each value of γ is $\gamma_{\rm NDC} = 1.018 \pm 0.043$ and $\gamma_{\rm PDC} = 1.014 \pm 0.042$. We find that they agree with that from the Landau theory (2.16), $\gamma = 1$, within the numerical error.

[3] Note that if the state with larger E were more stable, the transition point would

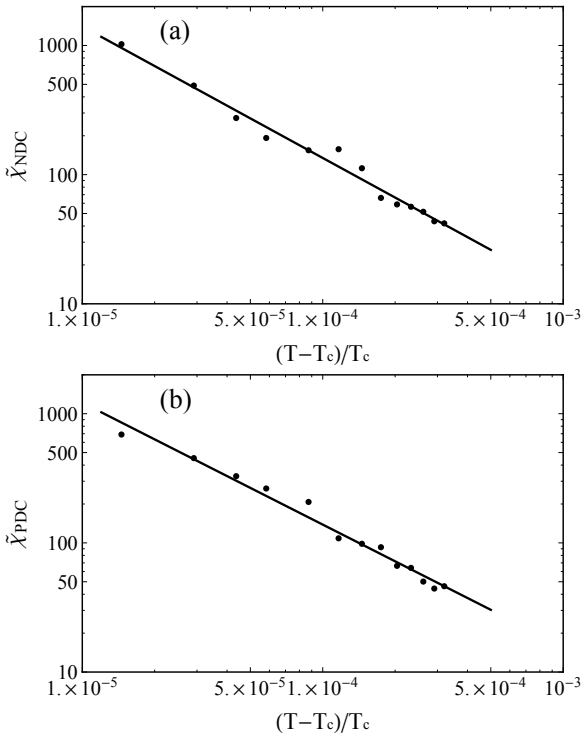

Figure 4.5: Critical behaviors of $\tilde{\chi}$ for $T > T_c$ (a) in the NDC phase and (b) in the PDC phase.

In addition, we evaluate the critical exponent γ for $T < T_c$. The counterpart of this situation for the equilibrium phase transition would be the liquid-vapor phase transition in which the susceptibility should be calculated along the critical isochore in the crossover region. From the analogy, we determine the line that corresponds to the critical isochore for our non-equilibrium phase transition. In analogy with the ferromagnet phase transition or the liquid-vapor transition, we choose this point as the inflection point in the J-σ curve. The phase diagram is shown in Fig. 4.6 and it is found that the inflection point for $T < T_c$ is nearly constant with $\sigma = \sigma_c = 0.0156$.

We show the relationship between the values of $\tilde{\chi}$ and the temperature along the $\sigma = \sigma_c$ line in Fig. 4.7. The numerical data gives $\gamma_{\rm crossover} = 1.022 \pm 0.025$. Furthermore, if we assume that $\gamma_{\rm NDC} = \gamma_{\rm PDC} = \gamma_{\rm crossover}$, we

be at C in Fig. 4.2. However, we cannot calculate $\tilde{\chi}$ at this point because $\partial E/\partial J$ always diverges there.

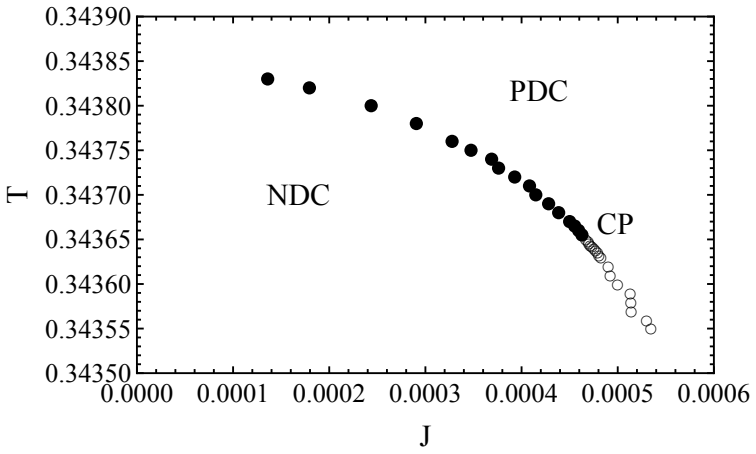

Figure 4.6: The phase diagram for our non-equilibrium phase transition. The filled circles are on the line of the first-order phase transition. The critical point (CP) is at $T_c = 0.34365$. The open circles are the inflection points where $\sigma = \sigma_c = 0.0156$.

find $\tilde{\chi}_{\rm crossover}/\tilde{\chi}_{\rm NDC} = 2.2 \pm 0.4$ and $\tilde{\chi}_{\rm crossover}/\tilde{\chi}_{\rm PDC} = 2.0 \pm 0.4$. These results agree with the fact that the critical amplitude ratio in the Landau theory is 2. The critical phenomena are exhibited in Fig. 4.7.

All of the above arguments go along with the chiral condensate instead of the conductivity. The obtained values of the corresponding critical exponents are $\gamma^{\rm NDC}_{\rm chiral} = 1.015 \pm 0.028$, $\gamma^{\rm PDC}_{\rm chiral} = 1.007 \pm 0.022$, and $\gamma^{\rm crossover}_{\rm chiral} = 0.979 \pm 0.029$. They agree with (2.16), again. The corresponding critical amplitude ratios are $\tilde{\chi}^{\rm crossover}_{\rm chiral}/\tilde{\chi}^{\rm NDC}_{\rm chiral} = 2.0 \pm 0.3$ and $\tilde{\chi}^{\rm crossover}_{\rm chiral}/\tilde{\chi}^{\rm PDC}_{\rm chiral} = 1.9 \pm 0.3$ which agree with 2 within the numerical error.

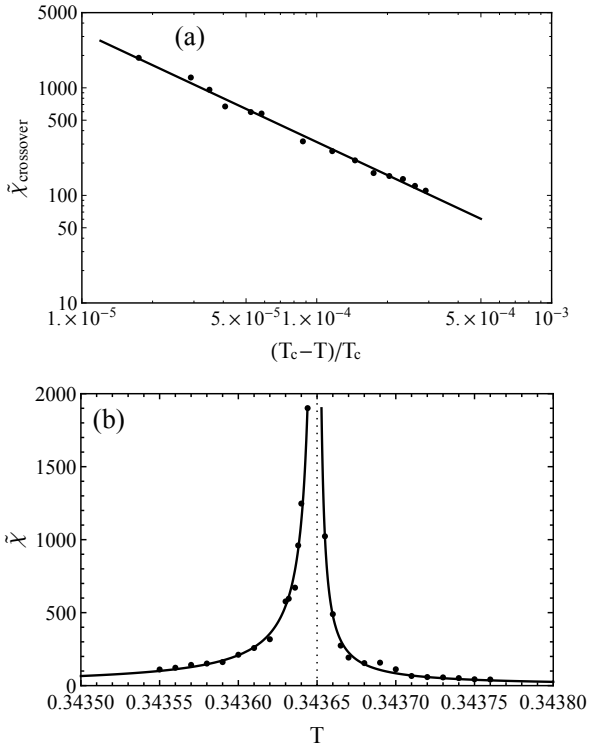

Figure 4.7: (a) Critical behavior of $\tilde{\chi}$ for $T < T_c$ and (b) the divergence of $\tilde{\chi}$ near the critical point.

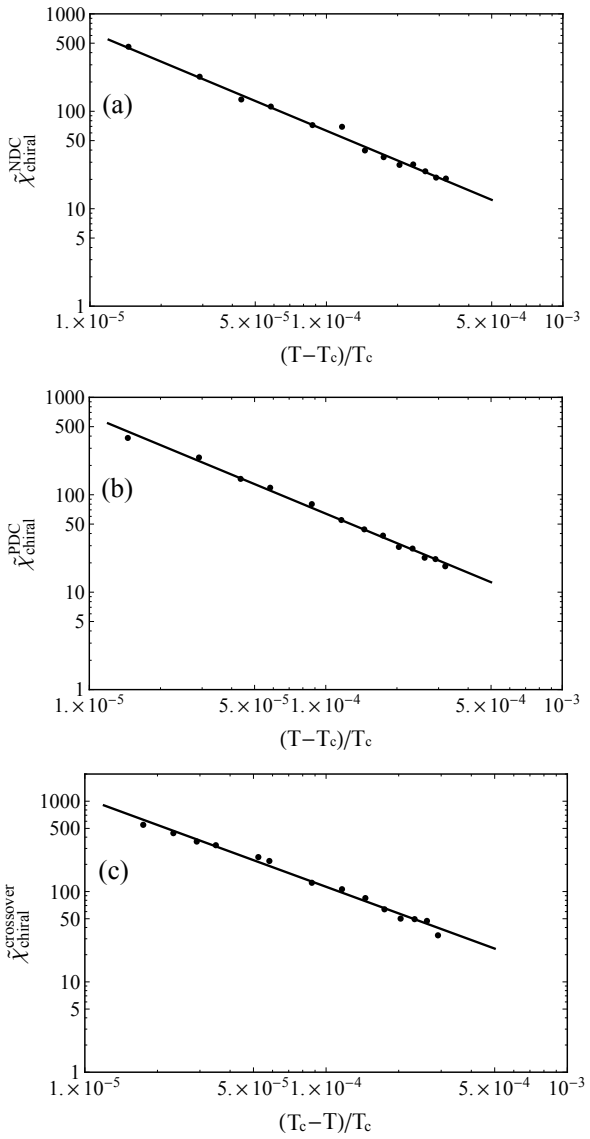

Figure 4.8: Critical behaviors of $\tilde{\chi}_{\rm chiral}$ (a) in the NDC phase, (b) in the PDC phase, and (c) in the crossover region.

Evaluation of α

The last but not least static critical exponent is α, which is related to the critical behavior of the specific heat. Although it is difficult to compute the specific heat in our model, there are models of equilibrium phase transitions in which a deviation of the law of rectilinear diameter gives the critical exponent α [30, 31, 32, 33]. Let us see how it goes for our case. If we assume that the foregoing method is valid in our system, we may define α as

$$\sigma_{\text{ave}} = \sigma_c + A|T - T_c|^{1-\alpha}, \tag{4.28}$$

where A is a constant, $\sigma_{\text{ave}} = (\sigma_{\text{NDC}} + \sigma_{\text{PDC}})/2$ and σ_c is the critical conductivity at $T = T_c$. In Fig. 4.9, we show the conductivities in the PDC phase, those in the NDC phase, and their averages. We obtain the value of the exponent $\alpha = 0.048 \pm 0.111$, which agrees with (2.16) of the Landau theory. We may define α_{chiral} as

$$\langle \bar{q}q \rangle_{\text{ave}} = \langle \bar{q}q \rangle_c + B|T - T_c|^{1-\alpha_{\text{chiral}}}, \tag{4.29}$$

where B is a constant, $\langle \bar{q}q \rangle_{\text{ave}} = \left(\langle \bar{q}q \rangle_{\text{NDC}} + \langle \bar{q}q \rangle_{\text{PDC}}\right)/2$ and $\langle \bar{q}q \rangle_c$ is the critical value of the chiral condensate. However, our numerical data shows that $B \simeq 0$: the values of the chiral condensates in each phase are arranged symmetrically with respect to the critical value, as is the case with the ferromagnet phase transition. For this reason, we cannot determine the value of α_{chiral} accurately in this manner. We leave more concrete definition of the critical exponent α for our phase transition to future work.[4]

4.1.5 Spectral function for the transverse fluctuation

So far, we have studied the static critical phenomena of the non-equilibrium phase transition. Furthermore, we are also interested in dynamical critical phenomena, In our case, it describes a characteristic behavior of the relaxation into the non-equilibrium steady state near the critical point instead of that into the equilibrium state.

To analyze the dynamical critical phenomena in our non-equilibrium phase transition, we compute the spectral function which is defined by

$$\chi_{\mu\nu}(k) = -2\,\text{Im}\,G^R_{\mu\nu}, \tag{4.30}$$

where $G^R_{\mu\nu}$ is the retarded Green function. The spectral function in the D3-D7 model has been studied in Refs. [34, 35]. Following these papers, we

[4] Note that it is not straightforward to define α by using the heat capacity, since the notion of the heat capacity in NESS is not clear.

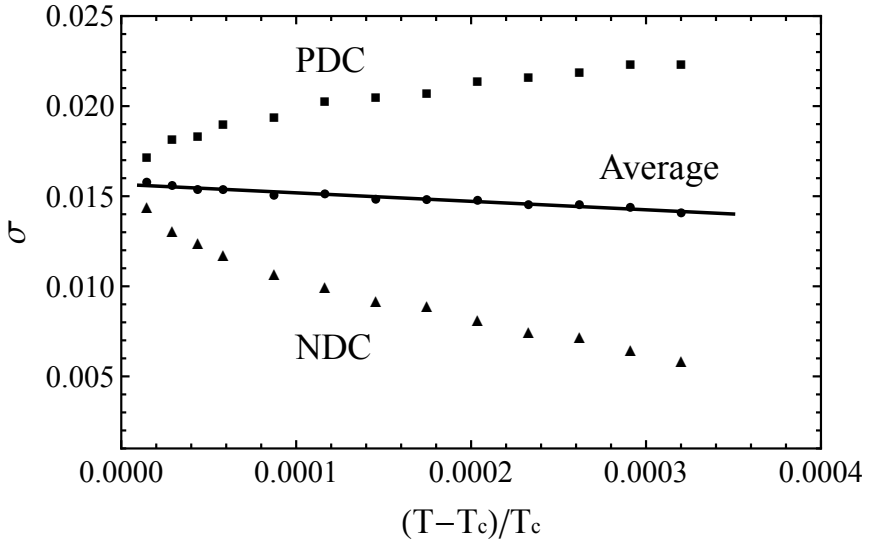

Figure 4.9: Critical behaviors of the conductivities in the NDC phase and the PDC phase and the average of them.

analyze the behavior of the spectral function near the critical point in our non-equilibrium phase transition.

Here we study the fluctuation of the gauge field perpendicular to the current density since its equation of motion does not couple to those of other fields. We employ the following ansatz for the gauge field

$$\begin{aligned} A_\mu dx^\mu &= A_x(z,t)dx + \delta A_\perp(z,t)dx_\perp \\ &= (-Et + a_x(z))\,dx + \epsilon e^{-i\omega t} a_\perp(z) dx_\perp, \end{aligned} \tag{4.31}$$

where $x_\perp$ is the coordinate perpendicular to x and ϵ is a small constant. If we expand the DBI Lagrangian in power of ϵ, we obtain the equation of motion for the perturbation from the term of order ϵ^2. The equation of motion becomes

$$a_\perp'' + \partial_z \log\left[\sqrt{-\gamma}\gamma^{\perp\perp}\gamma^{zz}\right] a_\perp' - \frac{\omega^2\gamma^{00}}{\gamma^{zz}} a_\perp = 0, \tag{4.32}$$

where $\gamma_{ab} = g_{ab} + F_{ab}$. In order to solve this equation of motion, we have to impose appropriate boundary conditions. We require the regularity of the solution at the black hole horizon. This condition can be achieved by

performing a Frobenius expansion. There are two possibilities of boundary conditions, namely outgoing or ingoing wave boundary conditions. Since the gauge field fluctuation must not propagate from the inside of the horizon, we choose the ingoing wave boundary condition which is given by

$$a_\perp(z) = (z_H - z)^{-\frac{i\omega}{4\pi T}} a_\perp^{\rm reg}(z), \tag{4.33}$$

where $a_\perp^{\rm reg}(z)$ is an analytic function at $z = z_H$. After we obtain the solution, the boundary action for the transverse fluctuation is written by

$$S_{\rm bdry} = -\frac{1}{2}\int d^4x\sqrt{-\gamma}\gamma^{\perp\perp}\gamma^{zz}a'_\perp(z)a_\perp(z)\Big|_{z\to 0}. \tag{4.34}$$

The Lorentzian prescription, which is proposed as a prescription to obtain the retarded Green function (see Ref. [36]), provides the Green function for the transverse gauge fluctuation

$$G_\perp^R = \sqrt{-\gamma}\gamma^{\perp\perp}\gamma^{zz}\,\frac{a'_\perp a_\perp^*}{|a_\perp|^2}\Big|_{z\to 0}. \tag{4.35}$$

Since the optical conductivity is related to the Green function as follows

$$\sigma_\perp(\omega) = -\frac{1}{\omega}\,{\rm Im}\,G_\perp^R(\omega), \tag{4.36}$$

we obtain the following relation

$$\chi_\perp(\omega) = -2\,{\rm Im}\,G_\perp^R = 2\omega\sigma_\perp(\omega). \tag{4.37}$$

In Fig. 4.10, we show the spectral function as a function of ω for several temperatures below T_c. As can be seen, several peaks are observed. In dual gauge field theory, these peaks can be considered as the excited state of the vector mesons without coupling to the electric current or the scalar mesons. We find that the width of each peak becomes narrower for higher temperature. If we write the retarded Green function for a single excited state as the following form

$$G^R(\omega) \sim \frac{1}{\omega - \omega_0 + i\Gamma}, \tag{4.38}$$

the spectral function has the form of

$$\chi(\omega) \sim \frac{\Gamma}{(\omega-\omega_0)^2 + \Gamma^2}. \tag{4.39}$$

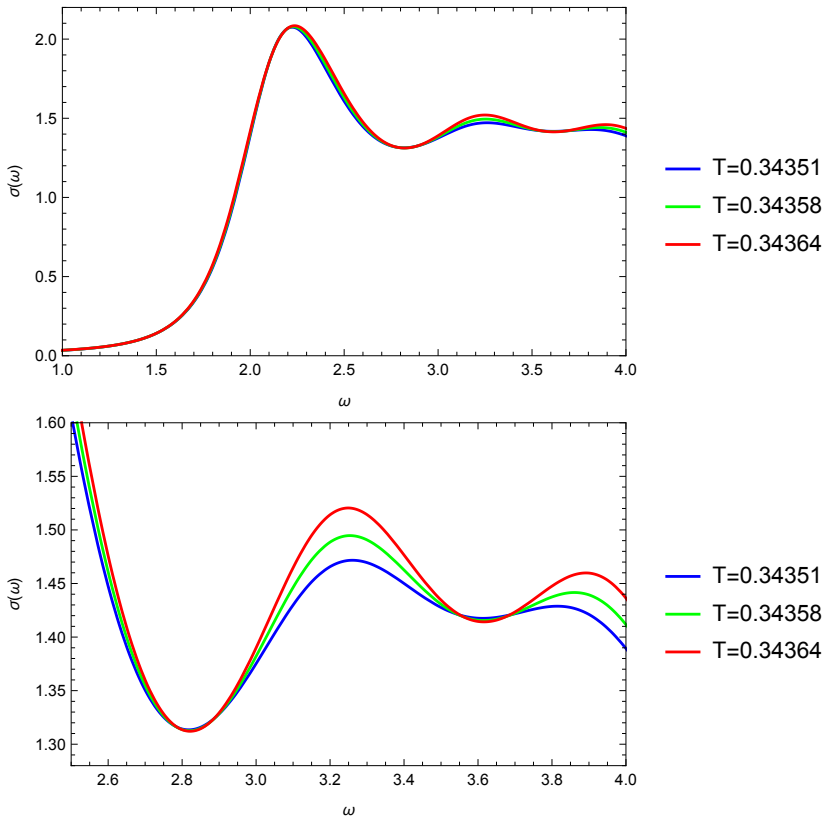

Figure 4.10: The spectral function for the transverse gauge fluctuation for several temperatures along the crossover line in the phase diagram. From bottom to up, the temperature for each plot is larger.

This form is a Lorentzian function which has the center of peak ω_0 and the peak width Γ. In general, the pole of the retarded Green function becomes complex and the imaginary part of that is related to the lifetime of a corresponding mode i.e. $\Gamma = 1/\tau$, where τ is the lifetime.

To analyze the lifetime of the vector meson near the critical point, we study the relation between the width of a peak of the spectral function and the temperature along the crossover line in the phase diagram shown in Fig. 4.6. For simplicity, we focus on the second excited mode as shown in the bottom figure plot of Fig. 4.10. Assuming the shape of this mode follows the Lorentzian function, we fit it for various temperatures. Fig. 4.12 shows numerical plots and linear fitting of the temperature dependence of Γ^2 near

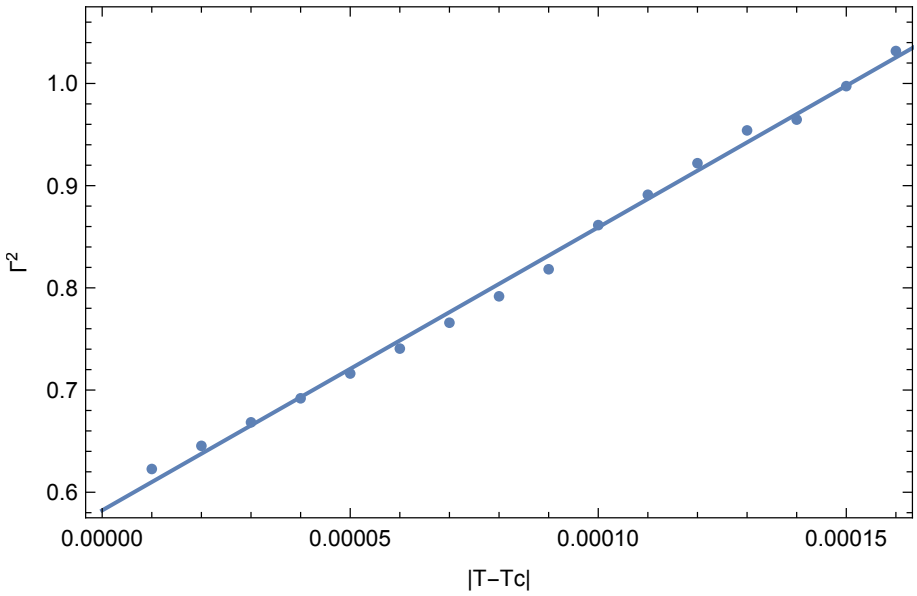

Figure 4.11: The temperature dependence of Γ^2 near the critical point.

the critical point. We find that Γ^2 is finite even in the critical temperature as shown in Fig. 4.11. In other words, we obtain the relation

$$\Gamma^2 - \Gamma_c^2 \propto |T - T_c|, \tag{4.40}$$

where Γ_c is the peak width at the critical point. Thus, we find that the lifetime of the vector meson does not diverge at the critical point.

If we compute the spectral function along the first-order phase transition line in the phase diagram, we find that each peak becomes much narrower for higher temperature as shown in Fig. 4.12. These results show that the vector mesons becomes more stable for higher temperature in the dual gauge field theory.

4.1.6 Conclusion and outlook

In this section, we study the non-equilibrium phase transition and critical phenomena in the D3-D7 conductor model. We find that the critical exponents of our non-equilibrium phase transition agree with those in the Landau theory: $\beta = 1/2$, $\delta = 3$, and $\gamma = 1$. The critical amplitude ratio of $\tilde{\chi}$ also agreed with that of the Landau theory. Our results satisfy the scaling laws

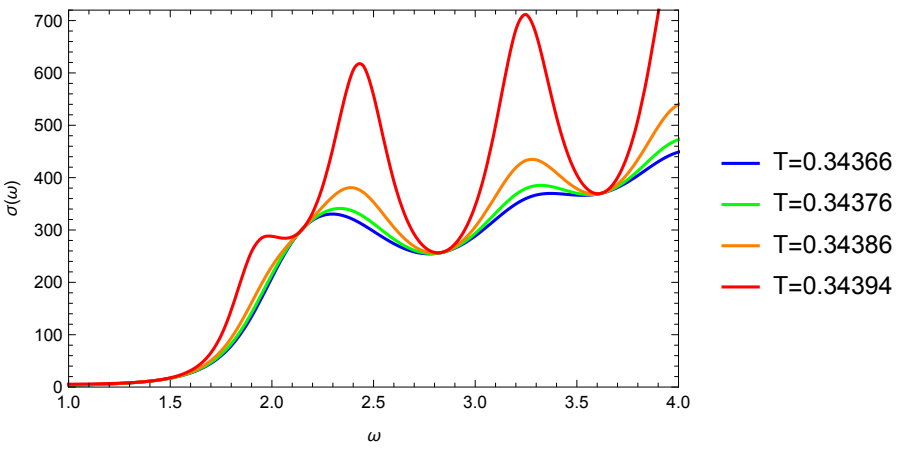

Figure 4.12: The spectral function for the transverse gauge fluctuations for several temperatures along the first-order phase transition line. From bottom to up, the temperature for each plot is larger.

such as the Widom scaling, $\gamma = \beta(\delta - 1)$, within the numerical error. In our definitions of the critical exponents, we assumed that $J - J_c$ plays the role of the magnetic field H in (2.4). We find that the critical exponent and the critical amplitude ratio of the susceptibility that we defined agree with those of the Landau theory of equilibrium phase transitions. Together with the results for β and δ, our results imply that the critical phenomena in the non-equilibrium phase transition in question have remarkable similarities with those in the Landau theory of equilibrium phase transition. Motivated with the dynamical critical phenomena, we compute the spectral function for the transverse gauge perturbation for the current density. Analyzing the relation between the width of a peak of the spectral function and the temperature near the critical point, we find that the Eq. (4.40) is satisfied in our non-equilibrium phase transitions.

Coming back to the questions raised in section 4.1.1, we obtained the answers to the questions of 1) and 2) as far as for the non-equilibrium phase transitions considered in this paper: we can define the susceptibility associated with J in a completely parallel manner to that in the Landau theory, and the susceptibility shows critical phenomena with $\gamma = 1$. For the question of 3), our results suggest that the critical exponents γ and δ associated with J may be formulated by using a theory similar to the Landau theory. However, further investigation is necessary to obtain a complete

answer.

In the future perspective, it would be interesting to compute other static critical exponents ν and η. To compute them, we have to consider the spatial dependence of the order parameter as explained in Section 2.3. We are also interested in the calculation of the specific heat. If we assume that it is given by the second-order derivative of the Hamiltonian with respect to the temperature, we might be able to compute the critical exponent α straightforwardly. Moreover, further study of the dynamical critical exponent would be required. As discussed in Section 4.1.5, the spectral function for the transverse gauge fluctuation does not have a characteristic behavior near the critical point. It might stem from the fact that the transverse gauge fluctuation decouples from the current density or the scalar field. Therefore, it is expected that we can observe some critical behaviors if we analyze the gauge fluctuation which couples to the other fields.

4.2 Spontaneous symmetry breaking in D3-D7 model

4.2.1 Introduction

In this section, we study another non-equilibrium phase transition which appears in the D3-D7 model. Particularly, we investigate a spontaneous symmetry breaking of $U(1)$ chiral symmetry of a strongly-coupled large-N_c gauge theory under the presence of an electric current density J and a magnetic field B perpendicular to the current. Employing the D3-D7 model, the gauge theory is $SU(N_c)$ $\mathcal{N} = 4$ supersymmetric Yang-Mills (SYM) theory in (3+1) dimensions with $\mathcal{N} = 2$ hypermultiplet. The quarks belong to the hypermultiplet whereas the particles that form the heat bath belong to the gluon sector of $\mathcal{N} = 4$ SYM. The D3-D7 model with both an electric field and a magnetic field has been studied in Ref. [37]. It has also been known that non-equilibrium phase transitions are observed in the presence of a magnetic field [38].

The quarks in our system are massless. This corresponds that we are dealing with gapless systems in condensed matter physics when the system has chiral symmetry. We find that the system exhibits first-order or second-order phase transitions of the chiral symmetry breaking, which corresponds to the appearance of the gap in the condensed matter system. A tricritical point exists between the line of the first-order phase transition and the second-order critical line. We stress that the newly discovered tricritical point is located at finite J in the NESS regime on the phase diagram, hence we call it as the non-equilibrium tricritical point. We present numerical

results for critical exponents at the critical points. Our results imply that the phase transitions of the present system are described by a Landau-like phenomenological model.

4.2.2 Setup

The setup is almost the same as that of the previous analysis. The geometry in the gravity side is a direct product of a five-dimensional AdS-Schwarzschild black-hole and an S^5 as given by Eqs. (4.1) and (4.2). In the former part, we use z ($0 \leq z \leq z_H$) for the radial direction, t and $\vec{x} = (x^1, x^2, x^3)$ for the coordinates in the (3+1) dimensions of the corresponding gauge theory. For simplicity, we set the AdS radius and the radius of S^5 to be 1 again. The dynamics of the D7-brane is described by the DBI action as given by Eq. (4.4).

Let us employ the following ansatz for the gauge fields:

$$A_1(t,z) = -Et + a_1(z), \tag{4.41}$$
$$A_2(x^1) = Bx^1 \tag{4.42}$$

and A_a for $a \neq 1, 2$ are zero. Then the non-vanishing components of the field strength F_{ab} are

$$F_{01} = -F_{10} = -E, \tag{4.43}$$
$$F_{12} = -F_{21} = B, \tag{4.44}$$
$$F_{1z} = -F_{z1} = a_1'(z). \tag{4.45}$$

From now, we denote x^1 by x for simplicity. The Lagrangian density is written by the same form as that in the previous section,

$$\tilde{\mathcal{L}}_{D7} = \sqrt{-\frac{g_{zz}}{g_{tt}g_{xx}}}\sqrt{\xi\chi}, \tag{4.46}$$

where

$$\xi = g_{xx}E^2 - |g_{tt}|g_{xx}^2 - |g_{tt}|B^2, \tag{4.47}$$
$$\chi = N|g_{tt}|g_{xx}^2\cos^6\theta - J^2. \tag{4.48}$$

Following the same discussion in the previous section, we require $\xi = 0$ and $\chi = 0$ simultaneously at the effective horizon. The first condition provides the explicit form of the effective horizon

$$z_*^4 = \left(F(e,b) - \sqrt{(F(e,b)-1)^2 - 1} - 1\right) z_H^4, \tag{4.49}$$

where

$$F(e,b) = 1 + e^2 - b^2 + \sqrt{\left(e^2 - b^2\right)^2 + 2\left(e^2 + b^2\right) + 1}. \tag{4.50}$$

Here e and b are defined as dimensionless quantities: $e = 2E/(\pi\sqrt{\lambda}T^2)$ and $b = 2B/(\pi\sqrt{\lambda}T^2)$, and λ is the 't Hooft coupling of the gauge theory. The second condition provides the explicit form of the current density

$$J^2 = N|g_{tt}|g_{xx}^2 \cos^6\theta(z_*). \tag{4.51}$$

The D7-brane embedding function $\theta(z)$ in the vicinity of the boundary can be expanded as the same form with Eq. (4.3).

4.2.3 Non-equilibrium phase transition

Here, we set $N = 1$ and $z_H = 1$ for simplicity. In order to solve the EOM for $\theta(z)$ numerically, we impose the boundary conditions (4.13) and (4.14) at the effective horizon. We solve the EOM numerically to obtain the solutions $\theta(z)$ in $\varepsilon \leq z \leq z_* - \varepsilon_{IR}$, where ε and ε_{IR} are cutoffs introduced to avoid numerical divergence at the boundary and the effective horizon, respectively.

Once $\theta(z)$ is obtained for each parameter, one can compute m_q and $\langle\bar{q}q\rangle$. Inversely, the configurations of the D7-brane and the parameters can be found for the fixed m_q. In this study, since we are interested in the system of massless quarks and the spontaneous chiral symmetry breaking, we take solutions for $m_q = 0$ by using the shooting method. In Fig. 4.13, we show the quark mass m_q as a function of the current density J. As can be seen, there are two possible solutions for $m_q = 0$ if the magnetic field is sufficiently large. We show the configurations of the D7-brane in Fig. 4.14. There exist two possible branches: the flat branch and the bending branch as shown in Fig. 4.14. The flat branch is a trivial solution: $\theta(z) = 0$. The bending branch is a non-trivial solution: $\theta(z) \neq 0$. These branches can be distinguished by the chiral condensate: $\langle\bar{q}q\rangle = 0$ in the flat branch, and $\langle\bar{q}q\rangle \neq 0$ in the bending branch. In other words, the chiral symmetry is preserved in the flat branch, whereas it is spontaneously broken in the bending branch.

To be more explicit, this spontaneous symmetry breaking is associated with an internal $U(1)_R$ symmetry in gauge theory side. On the other hand, in gravity side, the total system has an $SO(4) \times SO(2)$ symmetry in the flat branch. The $SO(4)$ group rotates four directions which are filled by the D7-brane but perpendicular to the D3-brane. The $SO(2)$ group rotates two directions which are perpendicular to the D7-brane. In the gravity description, the $SO(2)$ rotational symmetry is explicitly broken if the D7-brane

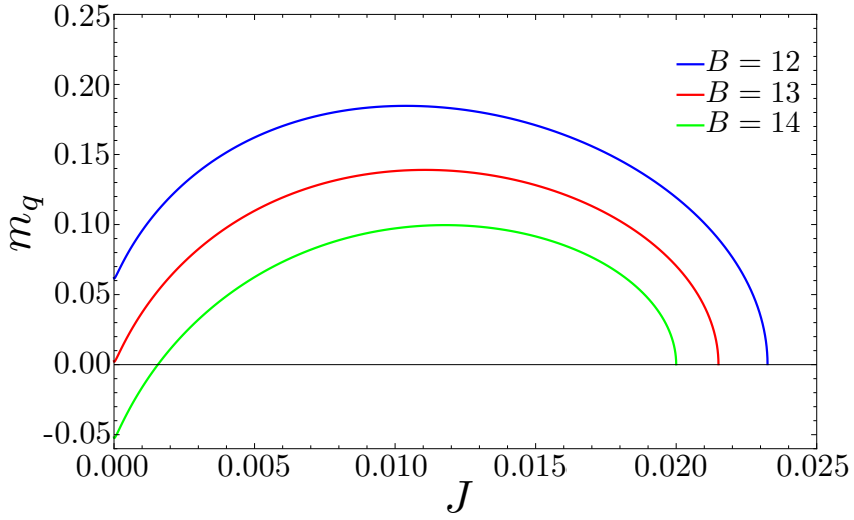

Figure 4.13: The numerical plots of J and m_q with $E = 0.1$ fixed for $B = 12$, $B = 13$, and $B = 14$. Each point is specified by $\theta(z_*)$, which takes 0 to $\pi/2$ (right to left).

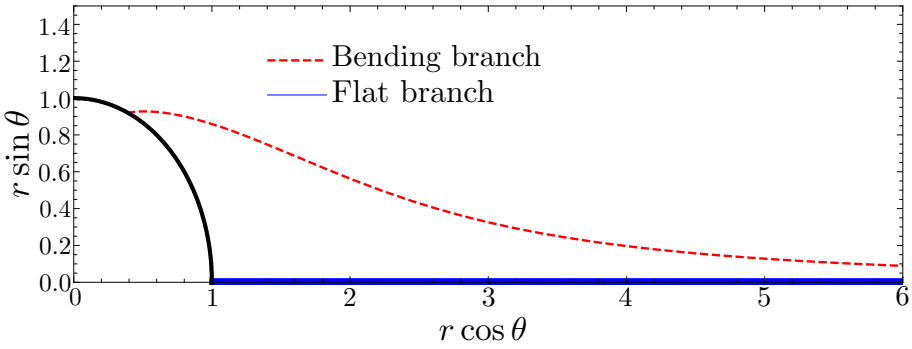

Figure 4.14: The D7-brane configurations of two possible branches for $E = 1$ and $B = 14$. The black solid line represents the black-hole horizon. The coordinate is changed following by $1/z^2 = r^2 + \sqrt{r^4 - 1}$. The black-hole horizon is located at $r = 1$, the effective horizon is located at $r = r_* > 1$, and the AdS boundary is located at $r = \infty$.

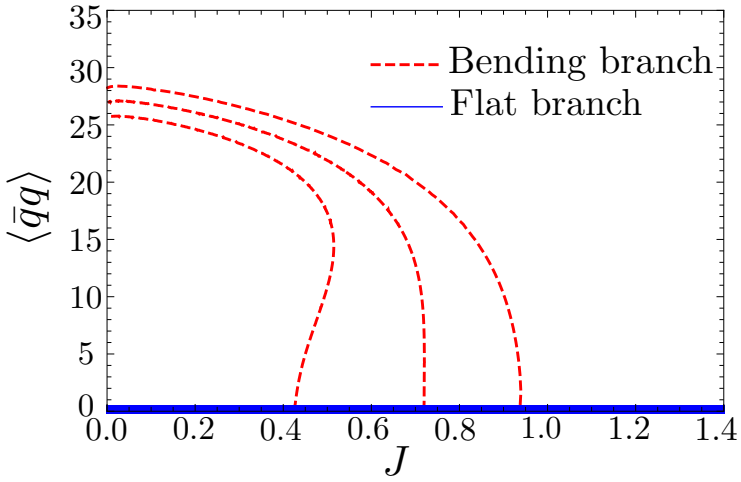

Figure 4.15: The behaviors of the chiral condensate $\langle \bar{q}q \rangle$ as a function of the current density J for $B = 19$, $B = 20$, and $B = 21$.

is separated from the D3-brane, which corresponds to a massive quark. In this study, however, the external fields and the current density induce the $SO(2)$ rotational symmetry breaking despite the quark mass is kept zero. In the dual gauge field theory, the $SO(2)$ symmetry corresponds to the mass generation by the $U(1)_R$ chiral symmetry. Since the spontaneous symmetry breaking in our setup makes the chiral condensate to be finite while a quark remains massless, this corresponds to the spontaneous chiral symmetry breaking. Compared to the previous studies on the chiral symmetry breaking in the AdS/CFT correspondence [39, 40, 41, 42, 43], the crucial difference in our study is that we consider chiral symmetry breaking in the NESS regime where $J \cdot E \neq 0$.

Fig. 4.15 shows the behaviors of the chiral condensate $\langle \bar{q}q \rangle$ and the current density J for various B. Note that if we choose the current density as a control parameter, there is a multivalued region where $\langle \bar{q}q \rangle$ has two or three possible values for a given J. In this region, we expect that only the most stable solution is realized.

In the following, we assume that the most stable solution has the lowest thermodynamic potential which is defined by the renormalized Hamiltonian of the D7-brane per unit volume with appropriate Legendre transformation

[28, 10]. In the present case, the Hamiltonian density is given by

$$\tilde{\mathcal{H}}_{D7} = g_{xx}\sqrt{-g_{tt}g_{zz}}\sqrt{\frac{J^2 + g_{tt}g_{xx}^2\cos^6\theta}{g_{tt}g_{xx}^2 + g_{tt}B^2 + g_{xx}E^2}}. \tag{4.52}$$

Then the thermodynamic potential is defined as

$$\tilde{F}_{D7}(B,J) = \lim_{\varepsilon\to 0}\left[\int_{\varepsilon}^{z_*} dz\tilde{\mathcal{H}}_{D7} - L_{\text{count}}(\varepsilon)\right], \tag{4.53}$$

where $L_{\text{count}}(\varepsilon)$ is the counterterm to renormalize the divergence at the boundary $z = 0$. The explicit form is given in [21] except for the finite counterterm we propose[5]. The details on the finite counterterm is shown in Appendix B.

If we compute the thermodynamic potential in each plot of Fig. 4.15, we find that as the magnetic field increases, the thermodynamic potential of the bending branch becomes smaller and it eventually becomes more stable than the flat branch. As a result, there is a transition between these two branches. We regard this transition as a non-equilibrium phase transition. More interestingly, when B becomes larger, the chiral condensate of the bending branch changes from a multi-valued function to a single-valued function, and thus the discontinuous jump of the chiral condensate becomes continuous transition. Hence, the first-order phase transition changes to the second-order phase transition by increasing B. In this paper, we choose the chiral condensate $\langle\bar{q}q\rangle$ as an order parameter.

4.2.4 Phase diagram

To summarize the foregoing discussions, we show the phase diagram of the non-equilibrium phase transitions in Fig. 4.16. The thick blue curve is the first-order phase transition line and the red curve is the critical line where the second-order phase transition occurs. Note that there are two specific points in the phase diagram: B_{gap} and B_{TCP}. For $B < B_{\text{gap}}$, stable solutions are only the flat branches. For $B > B_{\text{gap}}$, however, the bending branch can be stable. The other specific point B_{TCP} is the tricritical point (TCP) that is defined as a point where three coexisting phases become identical simultaneously. To see this in our system, it is necessary to consider another parameter dimension: the quark mass m_q which breaks the chiral symmetry explicitly. In analogy with the QCD phase diagram[6], we find that the (B, J)

[5] See also [25], for the holographic renormalization of probe D-branes.
[6] For example, see [44].

phase diagram with a finite mass contains a first-order phase transition line which terminates at a critical point. This can be understood by checking the behaviors of the chiral condensate as a function of the current density for small mass as shown in Fig. 4.17. Critical points for different masses form a critical line in the (B, J, m_q) phase diagram and the critical line terminates at $B_{\rm TCP}$ that is located on the slice of $m_q = 0$. We can extend the phase diagram into the negative mass region by performing a $U(1)$ chiral transformation. One finds that the extended phase diagram is symmetric under $m_q \to -m_q$. Hence, the three critical lines end at a single point $B_{\rm TCP}$. This is why $B_{\rm TCP}$ is regarded as the tricritical point.

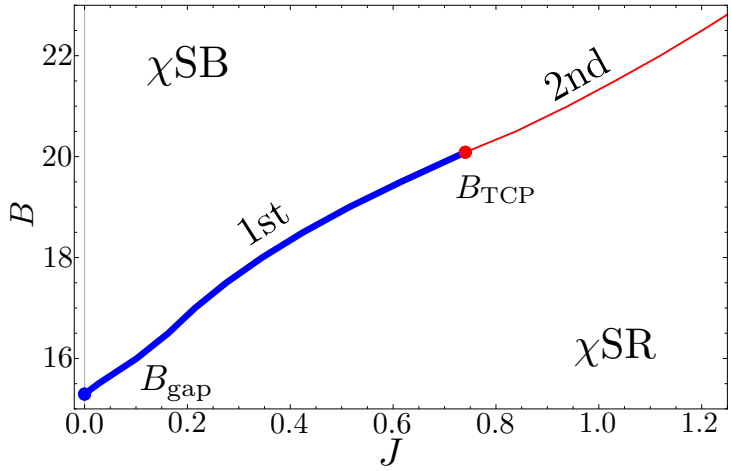

Figure 4.16: Phase diagram of the present system on the slice of $m_q = 0$. There are two specific points denoted by $B_{\rm gap}$ and $B_{\rm TCP}$. The first-order phase transitions occur along the thick blue curve and the second-order phase transitions occur along the red curve. These curves completely separate the phase with chiral symmetry restoration (χSR) and that with chiral symmetry breaking (χSB).

The detailed discussion for determining $B_{\rm gap}$ and $B_{\rm TCP}$ is the following. To determine the value of $B_{\rm gap}$, we have to find the specific value of B such that the minimum of the thermodynamic potential in the bending branch becomes lower than the maximum of the thermodynamic potential in the flat branch. We define the difference of them by

$$\Delta\tilde{F}_{D7} \equiv \min\left[\tilde{F}_{D7}^{\rm bend}\right] - \max\left[\tilde{F}_{D7}^{\rm flat}\right], \tag{4.54}$$

and we determine the value of $B_{\rm bend}$ such that $\Delta\tilde{F}_{D7} = 0$. As a result, we

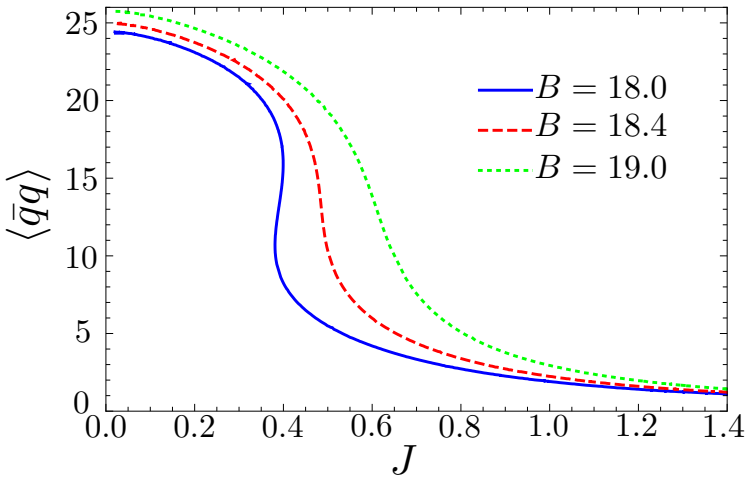

Figure 4.17: The behavior of the chiral condensate $\langle \bar{q}q \rangle$ at $m = 0.01$. When the magnetic field increases, the transition of the chiral condensate appears to be changed from first-order (solid line) to second-order (dashed line) and crossover (dotted line).

find $B_{\rm bend} \approx 15.294$ by linear fitting as shown in Fig. 4.18(a).

Next, we determine the value of $B_{\rm TCP}$ in the following method. First, we calculate the maximum values of J as a function of the thermodynamic potential $\tilde{F}_{D7}$ in the bending branch by quadratic fitting in the vicinity of the extremum point. If the value of $\tilde{F}_{D7}$ at that point is smaller than that of the flat branch, the point $(J, \tilde{F}_{D7})$ should be the transition point. Second, we calculate the intersection points of J-$\tilde{F}_{D7}$ curves of the flat branch and the bending branch. At $B = B_{\rm TCP}$, these points obtained by two different methods should be identical. Fig. 4.19 shows the schematic picture of our method to determine $B_{\rm TCP}$. In Fig. 4.19, thick curves denote the quadratic fitting of the actual plots of the bending branch near the maximum point. The thin curve is the plot of the flat branch. The cross marks and the circle marks show the maximum points of the quadratic fitting and the intersection point between two curves, respectively. The actual dates are shown in Fig. B.7 in Appendix B. Fig. 4.18 (b) shows the values of $\tilde{F}_{D7}$ in two different approaches for various B. This implies that there is a transition of the stable point from the maximum point to the intersection point at the specific value of $B = B_{\rm TCP}$. Consequently, the second-order phase transitions occur for $B \geq B_{\rm TCP}$. We find $B_{\rm TCP} \approx 20.086$ by linear fitting as

shown in Fig. 4.18 (b).

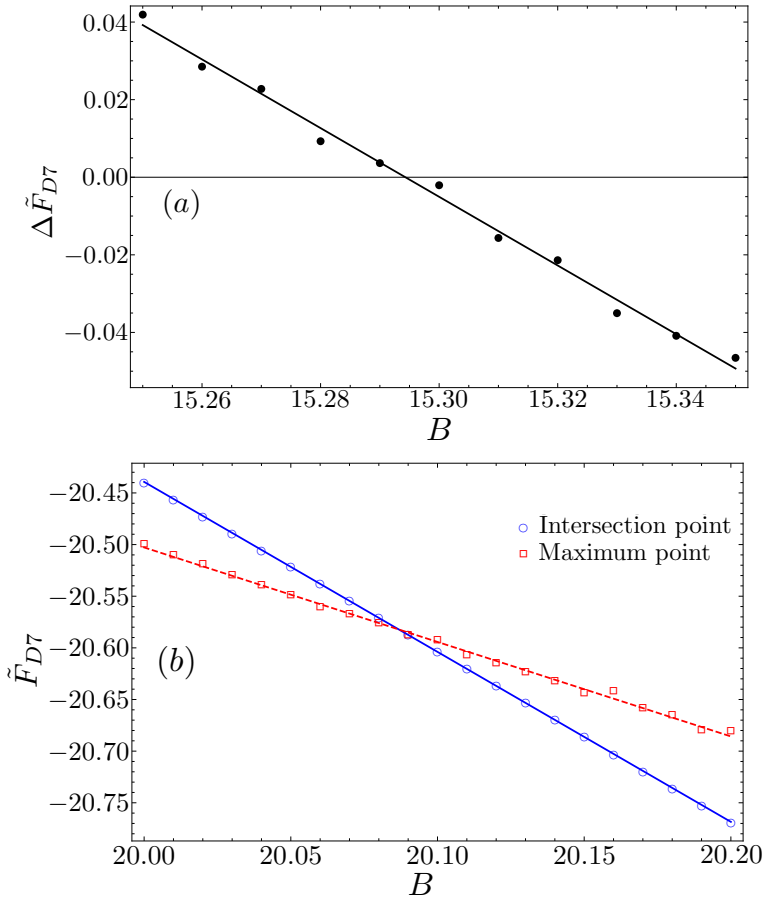

Figure 4.18: (a) The difference of the thermodynamic potentials in the flat branch and the bending branch for various B. We find $B_{\text{gap}} \approx 15.294$ by linear fitting. (b) The thermodynamic potentials calculated in two different approaches for various B. We find $B_{\text{TCP}} \approx 20.086$ by linear fitting.

4.2.5 Critical exponent

In the previous section, we found second-order phase transitions in our non-equilibrium system. To understand the critical phenomena, we analyze the critical exponents. Critical exponents are defined for the behavior of the order parameter near the critical point. In our analysis, we define the critical

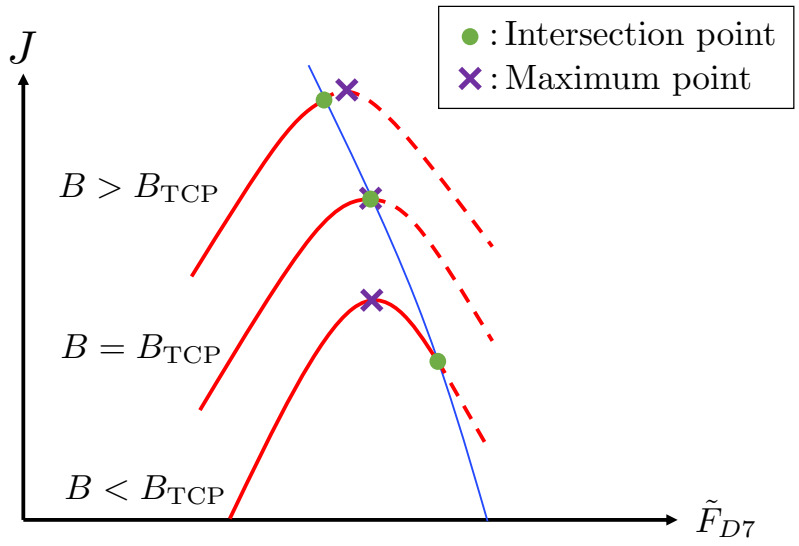

Figure 4.19: The schematic picture of our method to determine B_{TCP}. The thick curves denote the quadratic fitting of the bending branch near the maximum point, The thin curve is the plot of the flat branch.

exponent β as [7]

$$\langle \bar{q}q \rangle \propto (J_c - J)^{\beta}\,, \tag{4.55}$$

where J_c is the current density at the critical point. Fig. 4.20 shows the behaviors of $\langle \bar{q}q \rangle$ for $B > B_{\rm TCP}$, $B = B_{\rm TCP}$, and $B < B_{\rm TCP}$. As shown in the inset of Fig. 4.20, we find $\beta = 1/2$ for $B > B_{\rm TCP}$ and $\beta = 1/4$ for $B = B_{\rm TCP}$ within the numerical error by linear fitting.

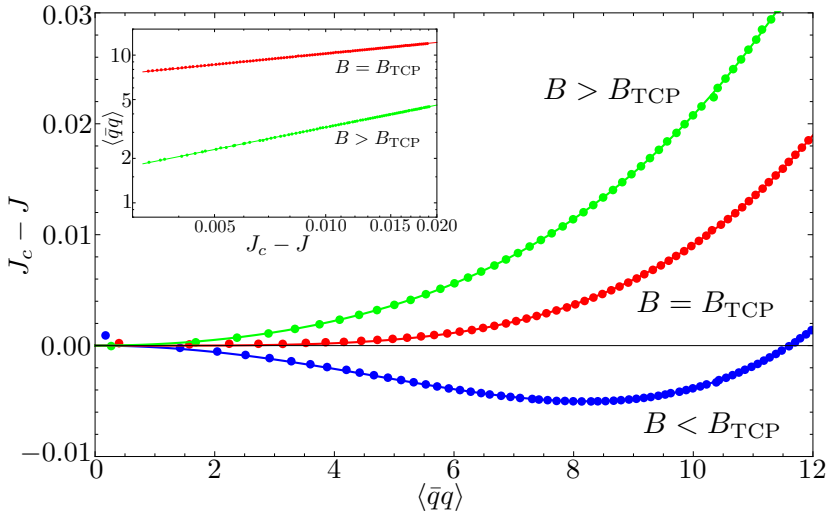

Figure 4.20: The current density $J_c - J$ as a function of the chiral condensate $\langle \bar{q}q \rangle$. The numerical plots and the lines obtained by non-linear fitting to the form of (4.59) for $B = 19.8$ (blue), $B = B_{\rm TCP}$ (red), and $B = 20.4$ (green) are shown. The inset shows numerical plots and linear fittings for $B = B_{\rm TCP}$ and $B = 30$.

4.2.6 Analytical approach

We show that the values of the critical exponents can be derived analytically as follows. Let us focus on the case for $B \geq B_{\rm TCP}$. In the language of the D7-brane configuration, $\theta(z)$ continuously changes from $\theta(z) = 0$ to $\theta(z) \neq 0$ when the chiral symmetry is broken in the second-order phase transition. This means that $\theta(z_*) \ll 1$ in the vicinity of the critical point.

[7] In Ref. [10], the critical exponent related to the chiral condensate and the current density is defined as $\left|\langle \bar{q}q \rangle - \langle \bar{q}q \rangle_c\right| \propto |J - J_c|^{1/\delta}$. In this study, we use β since the non-equilibrium phase transition in question is different.

Since $J = \sqrt{-g_{tt}g_{xx}^2}\Big|_{z_*} \cos^3\theta(z_*)$ is an even function of $\theta(z_*)$, J can be expanded as

$$J = J_c + a_2\theta(z_*)^2 + a_4\theta(z_*)^4 + \cdots , \tag{4.56}$$

where $a_i (i = 2, 4, \cdots)$ are coefficients that depend on z_*. Here we have used the fact that $J = J_c$ at the critical point where $\theta(z_*) = 0$. Note that J_c depend only on B.

It can be shown that the chiral condensate is an odd function of $\theta(z_*)$ as follows. For massless case, $\theta(z)$ in the vicinity of the boundary is expanded as

$$\theta(z) = -\frac{1}{2}\langle\bar{q}q\rangle z^3 + O(z^5). \tag{4.57}$$

Thus we find that the chiral condensate flips the sign if we flip the sign of $\theta(z)$. Therefore, the chiral condensate is an odd function of $\theta(z_*)$ which may be expanded as

$$\langle\bar{q}q\rangle = b_1\theta(z_*) + b_3\theta(z_*)^3 + \cdots , \tag{4.58}$$

where $b_i (i = 1, 3, \cdots)$ are coefficients that depend on z_*.

Suppose that $b_1 \neq 0$. In the case, the chiral condensate is *linear* in $\theta(z_*)$ in the vicinity of the critical point, and thus Eq. (4.56) gives

$$J_c - J = c_2\langle\bar{q}q\rangle^2 + c_4\langle\bar{q}q\rangle^4 + \cdots , \tag{4.59}$$

where c_2 and c_4 are some coefficients. The numerical results given in Fig. 4.20 suggest that $c_2 = \kappa(B - B_{\rm TCP})$ with $\kappa > 0$ and $c_4 > 0$, in the vicinity of $B = B_{\rm TCP}$. We have checked numerically that c_2 is indeed proportional to $B - B_{\rm TCP}$ and c_4 is a small positive value in the vicinity of the critical point. Then we obtain $\langle\bar{q}q\rangle \sim (J_c - J)^{1/2}$ for $B > B_{\rm TCP}$ and $\langle\bar{q}q\rangle \sim (J_c - J)^{1/4}$ for $B = B_{\rm TCP}$, respectively. The numerical results mensioned above for the critical exponents justify the above consideration. Therefore, we conclude that $\beta = 1/2$ for $B > B_{\rm TCP}$ and $\beta = 1/4$ for $B = B_{\rm TCP}$.

4.2.7 Conductivity

In Refs. [28, 10], it has been proposed that the conductivity $\sigma = J/E$ also plays a role of order parameter at least for the purpose of detection of the critical phenomena. From an experimental point of view, the measurement of conductivity is much easier than that of chiral condensate. Therefore, it is worth studying the phase transitions from the viewpoint of conductivity. Fig. 4.21 shows the J-E characteristics for various B. In terms of the conductivity, our non-equilibrium phase transitions are regarded as the transition

between the negative differential conductivity (NDC) phase and the positive differential conductivity (PDC) phase. They are corresponding to two branches, the bending branch and the flat branch, respectively. As shown in Fig. 4.21, the transition between the PDC phase and the NDC phase is also the second-order phase transition along the critical line and the first-order phase transition below $B_{\rm TCP}$. At the tricritical point, $\partial E/\partial J \to \infty$, which is similar behavior to that of the chiral condensate in Fig. 4.15. This shows that the chiral symmetry breaking is closely related to the transition between the PDC phase and the NDC phase. In other words, our results suggest that our non-equilibrium phase transitions and the tricritical point will be experimentally observed as transitions between the NDC phase and the PDC phase in a strongly coupled system with a constant current.

4.2.8 Conclusion and outlook

We studied the phase structure associated with the chiral symmetry of the current-driven NESS by using the AdS/CFT correspondence. We have discovered the current-driven tricritical point. If we define the critical exponent β as $\langle \bar{q}q \rangle \propto (J_c - J)^\beta$, we obtain $\beta = 1/2$ on the critical line and $\beta = 1/4$ at the tricritical point. These values of the critical exponents agree with those of the Landau theory for equilibrium systems. We also have revealed that similar behaviors are found if we consider the conductivity as the order parameter. Then, we propose that this type of non-equilibrium phase transitions and the current-driven tricritical point may be detected in a system consisting of gapless chiral fermions, such as a Weyl semimetal, with a constant current. We hope the results presented here provide clues to reveal the universal properties of some classes of the NESS.

We have some future outlooks. It is interesting to investigate if other critical exponents also agree with those of the Landau theory or not. Moreover, according to the Nambu-Goldstone theorem, if the continuous symmetry is spontaneously broken, the massless mode, so-called Nambu-Goldstone mode, must appear in the excitations. In our case, a fluctuation along one of rotational directions perpendicular to the D7-brane, which corresponds to the pseudo-scalar meson in the dual gauge field theory [45], should be the Nambu-Goldstone mode. On the other hand, it is expected that the pseudo-scalar meson has finite lifetime due to the holographic meson melting [46]. It is great interest of whether the Nambu-Goldstone mode which has finite lifetime appears.

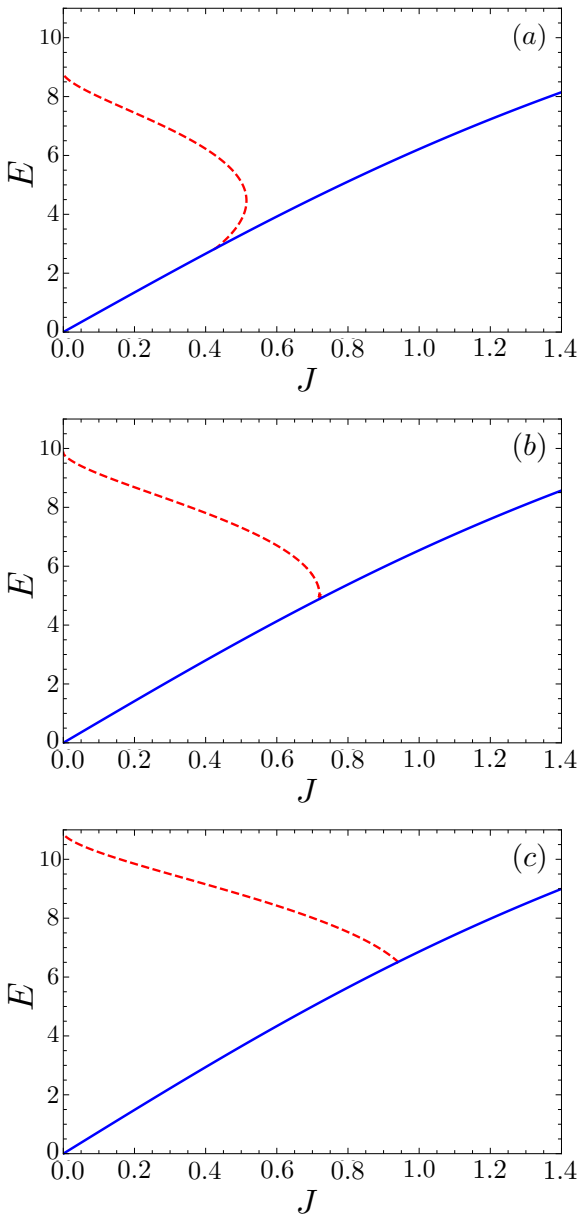

Figure 4.21: The J-E characteristics for (a) $B = 19$, (b) $B = 20$, and (c) $B = 21$.

Chapter 5

Summary and future perspectives

In this last chapter, we would like to summarize our works. In this thesis, we have studied non-equilibrium phase transitions and critical phenomena in the framework of the gauge/gravity duality. Employing the D3-D7 model, we have focused on the $\mathcal{N} = 4$ $SU(N_c)$ supersymmetric Yang-Mills theory coupled to flavor fields preserving $\mathcal{N} = 2$ supersymmetry as the dual field theory. Applying the electric field on the probe D7-brane, the NESS with a constant electric current is realized in the dual field theory. The system exhibits the non-linear J-E characteristics, which results in the non-equilibrium phase transition.

In Section 4.1, we have presented the analysis of critical phenomena of the non-equilibrium phase transition. We have assumed that the control parameter is the heat bath temperature T and the current density J is considered as an external field. Then, the phase diagram can be drawn in the parameters (T, J) as shown in Fig. 4.6. We have obtained the values of critical exponents as follows:

$$\beta = 1/2, \quad \delta = 3, \quad \gamma = 1, \quad \alpha = 0.$$

Here, we have confirmed that these are satisfied whichever we have chosen the conductivity $\sigma = J/E$ and the chiral condensate $\langle \bar{q}q \rangle$ as an order parameter within numerical errors. Moreover, we have found that the critical amplitude is equal to two. All of these results agree with those of the Landau theory in equilibrium phase transitions.

In Section 4.2, we have investigated another non-equilibrium phase transition in the presence of both the current density J and the transverse mag-

netic field B. In this setup, we have focused on the massless quark and regarded the chiral condensate $\langle \bar{q}q \rangle$ as an order parameter. We have studied the phase diagram for (J, B) with temperature fixed. We have found that there are both the first-order phase transition line and the second-order phase transition line in the phase diagram as shown in Fig. 4.16. Moreover, this non-equilibrium phase transition is associated with the $U(1)$ chiral symmetry breaking in the dual field theory. Considering the additional parameter, the quark mass m_q, we have revealed that there is the tricritical point $(J_{\rm TCP}, B_{\rm TCP})$ in the phase diagram. To the best of our knowledge, this type of current-driven tricritical point has not been reported. Furthermore, we have found that the critical exponent β is given by

$$\begin{aligned} \beta &= 1/2 \qquad \text{(critical point)}, \\ \beta &= 1/4 \qquad \text{(tricritical point)}, \end{aligned}$$

which agree with those of the Landau theory again.

Our results imply that the non-equilibrium phase transitions of the present model might be described by the Landau-like phenomenological model as suggested by agreement of the critical exponents. Additionally, since our non-equilibrium phase transitions are associated with the nonlinear conductivity, it is possible to realize them and detect the tricritical point experimentally. In other words, our results propose the existence of a current-driven tricritical point associated with the $U(1)$ chiral symmetry breaking in the NESS. We hope that our findings provide some clues for understanding the universal features of the NESS.

To end this thesis, we will present some issues left for future exploration. Firstly, as we mentioned in the previous section, we are interested in the other critical exponents including dynamical critical exponents. This check will ensure the agreement with critical phenomena in equilibrium phase transitions. Secondly, our primary question is whether the system in a NESS has a free energy as defined in equilibrium systems. It would be interesting to consider a Landau-like phenomenological model by using our results of critical phenomena.

Appendix A

Anti-de Sitter spacetime

In this appendix, we discuss AdS spacetime and review some properties of that. Before we consider the AdS spacetime, let us consider an easy example: two-dimensional sphere S^2. The two-dimensional sphere is defined by a plane which satisfies

$$X^2 + Y^2 + Z^2 = L^2 \tag{A.1}$$

in the three-dimensional Euclid space given by

$$ds^2 = dX^2 + dY^2 + dZ^2, \tag{A.2}$$

where X, Y, and Z are the coordinates of the three-dimensional Euclid space. L is the radius of S^2. The plane (A.1) is satisfied by considering the polar coordinates

$$\begin{aligned} X &= L\sin\theta\cos\phi, \\ Y &= L\sin\theta\sin\phi, \\ Z &= L\cos\theta. \end{aligned}$$

In the polar coordinates, the metric of S^2 is written by

$$ds^2 = L^2\left(d\theta^2 + \sin^2\theta d\phi^2\right). \tag{A.3}$$

We easily find that S^2 has the $SO(3)$ symmetry. S^2 has a positive curvature and Ricci scalar is given by

$$R = \frac{2}{L^2}. \tag{A.4}$$

Next, let us consider a two-dimensional hyperbolic space H^2, which is defined by a plane satisfying

$$-Z^2 + X^2 + Y^2 = -L^2. \tag{A.5}$$

The hyperbolic space H^2 can be embedded in the three-dimensional Minkowski space which is given by

$$ds^2 = -dZ^2 + dX^2 + dY^2. \tag{A.6}$$

The plane (A.5) is satisfied by considering the following coordinates

$$\begin{aligned} X &= L\sinh\rho\cos\phi, \\ Y &= L\sinh\rho\sin\phi, \\ Z &= L\cosh\rho. \end{aligned}$$

In this coordinates, the metric of H^2 is written by

$$ds^2 = L^2\left(d\rho^2 + \sinh^2 d\phi^2\right). \tag{A.7}$$

In the case of H^2, the metric has the $SO(1,2)$ symmetry, which corresponds to the Lorentz symmetry in (2+1)-dimensional Minkowski spacetime. H^2 has a negative curvature and Ricci scalar is given by

$$R = -\frac{2}{L^2}. \tag{A.8}$$

Furthermore, we consider the spacetime which has two directions of time. The AdS_2 is defined by a plane which satisfies

$$-X^2 - Y^2 + Z^2 = -L^2, \tag{A.9}$$

where L is referred to as *the AdS radius*. AdS_2 is embedded in the spacetime

$$ds^2 = -dX^2 - dY^2 + dZ^2. \tag{A.10}$$

In a similar way, the plane (A.9) is satisfied by considering the following coordinates

$$\begin{aligned} X &= L\cosh\rho\cos\tau, \\ Y &= L\cosh\rho\sin\tau, \\ Z &= L\sinh\rho. \end{aligned} \tag{A.11}$$

This coordinates (ρ, τ) are referred to as *the global coordinate*. In the global coordinates, the metric of AdS_2 is written by

$$ds^2 = L^2 \left(-\cosh^2 \rho d\tau^2 + d\rho^2 \right), \tag{A.12}$$

where ρ and τ are defined in the range of $0 < \rho < \infty$ and $0 < \tau < 2\pi$, respectively. Since the time coordinate τ is periodic, we take the universal cover with $\tau \in \mathbb{R}$. We find that the AdS_2 spacetime has $SO(2,1)$ symmetry. Note that the AdS_2 spacetime has a single direction of time, while the original spacetime has two directions of time.

For convenience, there are several coordinates to describe the AdS spacetime. If we parametrize

$$r = \sinh \rho, \tag{A.13}$$

the AdS_2 metric (A.12) is rewritten by

$$\frac{ds^2}{L^2} = -(r^2+1)d\tau^2 + \frac{dr^2}{r^2+1}, \tag{A.14}$$

where coordinates (τ, r) are defined in the range of $-\infty < \tau < \infty$ and $0 < r < \infty$, respectively.

Another choice of the coordinates is the so-called *Poincarè coordinate* whose parametrization is given by

$$\begin{aligned} X &= Lut, \\ Y &= \frac{1 + u^2(L^2 - t^2)}{2u}, \\ Z &= \frac{1 - u^2(L^2 + t^2)}{2u}, \end{aligned}$$

where coordinates (t, u) are defined in the range of $-\infty < t < \infty$ and $0 < u < \infty$, respectively. In the poincarè coordinate, the AdS_2 metric is written by

$$\frac{ds^2}{L^2} = -u^2 dt^2 + \frac{du^2}{u^2}. \tag{A.15}$$

In this coordinate, the AdS boundary is located at $u = \infty$.

In general $(p+2)$-dimensional spacetime, the metric of AdS_{p+2} for the global coordinates is written by

$$\frac{ds^2}{L^2} = -(r^2+1)d\tau^2 + \frac{dr^2}{r^2+1} + r^2 d\Omega_p^2, \tag{A.16}$$

where $\sum_{i=1}^{p+2} \Omega_i^2 = 1$. On the other hand, in the Poincarè coordinates, the metric is written by

$$\frac{ds^2}{L^2} = u^2 \left(-dt^2 + d\vec{x}^2\right) + \frac{du^2}{u^2}, \tag{A.17}$$

where $\vec{x}$ is the coordinate of the p-dimensional space. Fig. A.1 shows the AdS_{p+2} spacetime in the global coordinate and the Poincarè coordinate. In the global coordinate, the boundary geometry is given by $R^t \times S^p$. On the other hand, in the Poincarè coordinate, the boundary geometry is given by $R^{1,p}$, which corresponds to the p-dimensional Minkowski spacetime.

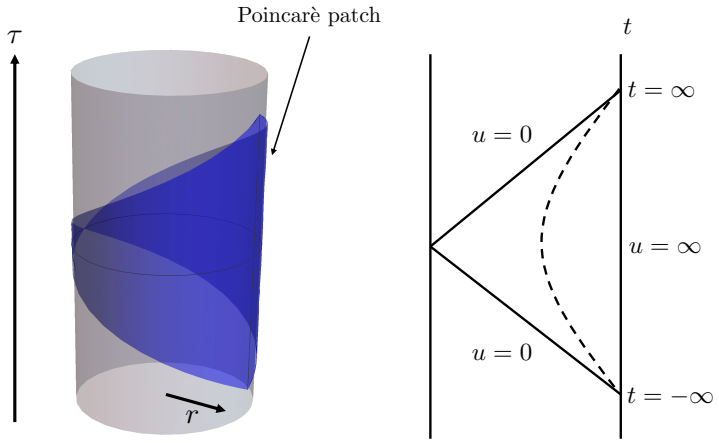

Figure A.1: The AdS spacetime in the global coordinate (left) and in the Poincarè coordinate. The dashed curve in the Poincarè coordinate denotes the line with $r = \text{const}$.

Appendix B

Counterterms for themodynamic potential

In this appendix, we show the explicit form of the counterterm in Eq. (4.53) in Section 4.2 and the behaviors of the thermodynamic potential.

$L_{\rm count}(\varepsilon)$ in Eq. (4.53) is the counterterm that renormalize the divergence at the boundary $z = 0$. $L_{\rm count}(\varepsilon)$ consists of four components

$$L_{\rm count}(\varepsilon) = L_1 + L_2 + L_f + H_F, \tag{B.1}$$

where the first three terms are given in [21]:

$$L_1 = \frac{1}{4}\sqrt{-\det\gamma_{ij}} = \frac{1}{4}\varepsilon^{-4}, \tag{B.2}$$

$$L_2 = -\frac{1}{2}\sqrt{-\det\gamma_{ij}}\theta(\varepsilon)^2 = -\frac{1}{2}\varepsilon^{-2}\theta_0^2, \tag{B.3}$$

$$L_f = \frac{5}{12}\sqrt{-\det\gamma_{ij}}\theta(\varepsilon)^4 = \frac{5}{12}\theta_0^4. \tag{B.4}$$

Here γ_{ij} is the induced metric on the $z = \varepsilon$ slice. We aim to determine the explicit form of H_F for the massless systems of the D3-D7 model. As discussed in [28], H_F is essentially given by the Legendre transform of the L_F presented in [21]. However, the L_F in [21] in the present notation is

$$L_F = -\frac{1}{2}F^2\log\varepsilon, \tag{B.5}$$

and the argument of the logarithm is not explicitly dimensionless. We claim that the argument of the logarithm should be made dimensionless by using F^2 for the present work.

To specify the explicit form of L_F for us, we consider the simplest case. Since the renormalization of UV divergence is not affected by the macroscopic setup, we consider the case that the current density is absent and the system is in equilibrium. We achieve this by introducing only a magnetic field, but we write $F^2 = 2(B^2 - E^2)$ to make the expressions Lorentz invariant. Then the Hamiltonian gives the equilibrium free energy. Note that this is equal to (-1) times the Lagrangian when the system is static and E is absent. We take the zero-temperature limit, and we set $m = 0$.

Let us evaluate the Lagrangian explicitly. We introduce coordinates (ρ, y) given by $1/z^2 = \rho^2 + y^2$ *i.e.*, $\rho = \cos\theta(z)/z$ and $y = \sin\theta(z)/z$. If we expand $\theta(z)$ near the AdS boundary, we find that the value of y at the boundary gives the mass of the charged particles: $y \to m$ at $\rho \to \infty$. Notice that ρ has a mass dimension in our convention.

Then the Lagrangian of D7-brane (per unit volume) is given by

$$L_{D7} = \int_0^\infty d\rho\, \rho^3 \sqrt{1 + \frac{F^2}{\rho^4}}. \tag{B.6}$$

If we introduce cutoffs $\rho_{\rm max}$ and $\rho_{\rm min}$ at the boundary and the origin, respectively, the Lagrangian density is rewritten as

$$\begin{aligned} L_{D7} &= \int_{\rho_{\rm min}}^{\rho_{\rm max}} d\rho\, \rho^3 \sqrt{1 + \frac{F^2}{\rho^4}} \\ &= \left[\frac{1}{4}\rho^2\sqrt{F^2+\rho^4} + \frac{1}{4}F^2 \log\left(\rho^2 + \sqrt{F^2+\rho^4}\right)\right]_{\rho_{\rm min}}^{\rho_{\rm max}} \\ &\simeq \frac{1}{4}\rho_{\rm max}^2\sqrt{F^2+\rho_{\rm max}^4} + \frac{1}{4}F^2 \log\frac{\rho_{\rm max}^2 + \sqrt{F^2+\rho_{\rm max}^4}}{\rho_{\rm min}^2 + \sqrt{F^2+\rho_{\rm min}^4}} \\ &\simeq \frac{\rho_{\rm max}^4}{4} + \frac{F^2}{8}\log\left(\frac{4e}{F^2}\rho_{\rm max}^4\right), \end{aligned} \tag{B.7}$$

where e is the Napier number. Notice that $\rho_{\rm max}$ is related to the UV cutoff $z = \varepsilon$ in the z coordinate as $\rho_{\rm max} = 1/\varepsilon$. Here we approximate

$$\sqrt{F^2+\rho_{\rm max}^4} \simeq \rho_{\rm max}^2\left(1 + \frac{F^2}{2\rho_{\rm max}^4}\right), \tag{B.8}$$

and ignore the terms that go to zero in the limit $\rho_{\rm max} \to \infty$ and $\rho_{\rm min} \to 0$. We note that for finite F^2, $\rho_{\rm min}$ is harmlessly taken to be 0. The first term is renormalized by L_1, and the second term may be renormalized by

$$L_F = \frac{F^2}{2}\log\rho_{\rm max}, \tag{B.9}$$

given in [21]. However, in this case, there is a remaining finite contribution from the second term which causes divergence in the susceptibility

$$\left.\frac{\partial^2 H}{\partial B^2}\right|_{B=0,E=0} = -\left.\frac{\partial^2 L_{D7}}{\partial B^2}\right|_{B=0,E=0} \tag{B.10}$$

at the zero-field limit. In order to avoid the divergence in the susceptibility, we need to subtract the finite contribution together with the logarithmic UV divergence. We have an ambiguity to choose the finite contribution which does not cause the divergence in the susceptibility. We set this finite term so that the susceptibilities are zero for the vacuum state where $T = F^2 = 0$. Then one finds that the second term in (B.7) has to be subtracted entirely. We do not put any further finite term which is independent of F^2, because we need to make the Hamiltonian zero for the supersymmetric setup of $T = F^2 = 0$. Then we conclude that our L_F should be

$$L_F = \frac{F^2}{8}\log\left(\frac{4e\rho_{\max}^4}{F^2}\right) = -\frac{F^2}{8}\log\left(\frac{F^2\varepsilon^4}{4e}\right). \tag{B.11}$$

Now, the argument in the logarithm is made dimensionless. So far, we have switched off the electric field. However, E^2 can be safely revived in F^2 since the renormalization must be made in a Lorentz invariant way.

The counterterm for the Hamiltonian is straightforwardly obtained by performing Legendre transformation

$$H_F = -L_F + E\frac{\partial L_F}{\partial E}. \tag{B.12}$$

The result is

$$H_F = \frac{F_{\rm E}^2}{8}\log\left(\frac{F^2\varepsilon^4}{4e}\right) + \frac{E^2}{2}, \tag{B.13}$$

where $F_{\rm E}^2 = 2(E^2 + B^2)$. One finds that the last term comes from the Legendre transformation.

We compute the renormalized thermodynamic potential using the counterterms given above. The behaviors of the thermodynamic potential as a function of J for several values of B are shown in the left column of Fig. B.7. In Fig. B.7, we also show the J-E characteristics and $\langle\bar{q}q\rangle$ as a function of J. The arrows in the plots indicate the first-order transition point based on the assumption that the stable state has the lowest thermodynamic potential. As we mention in the main text, when B is small, the flat branch is always favored as shown in Fig. B.7 for $B = 14$. However, if we increase

B, the bending branch gradually becomes stable as shown in Fig. B.7 for $B = 16$. This indicates that the first-order phase transition appears at the specific value of $B = B_{\mathrm{gap}}$. For larger B, the bending branch is always stable compared to the flat branch as shown in Fig. B.7 for $B = 18$, $B = 20$, and $B = 22$. Furthermore, the bending branch becomes single-valued for $B = 22$. This indicates that the first-order phase transition is changed to the second-order phase transition at the specific point $B = B_{\mathrm{TCP}}$.

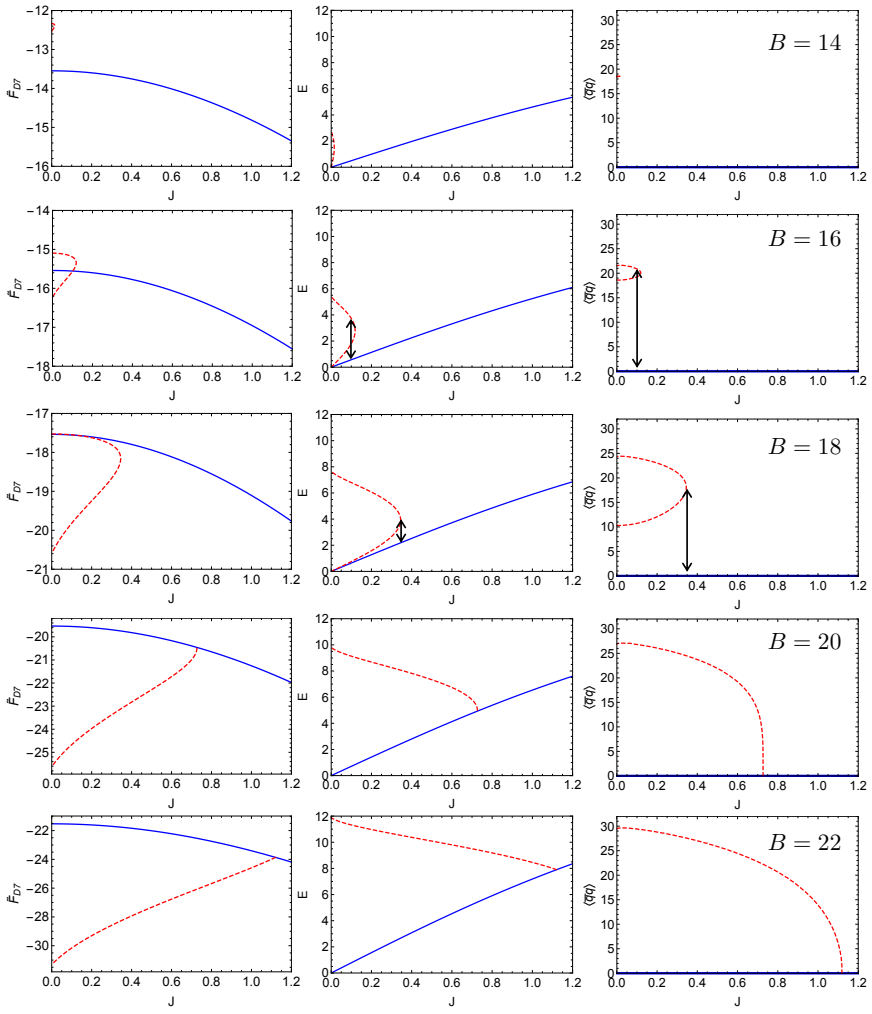

Figure B.7: Figures in the left column show the thermodynamic potential $\tilde{F}_{D7}$ as a function of J for $B = 14$, $B = 16$, $B = 18$, $B = 20$, and $B = 22$ from top to bottom. In the middle column, J-E characteristics are shown for each value of B. In the right column, we show $\langle \bar{q}q \rangle$ as a function of J for each value of B. The red dashed plots denote the bending branch and the solid blue plots denote the flat branch. The arrows in the plots indicate the points where the first-order phase transition occurs.

Bibliography

[1] H. Hinrichsen, "Nonequilibrium Critical Phenomena and Phase Transitions into Absorbing States," Adv. Phys. **49**, 815, (2000) [cond-mat/0001070].

[2] S. Lubeck, "Universal Scaling Behavior of Non-Equilibrium Phase Transitions," Int. J. Mod. Phys. B **18**, 3977 (2004) [cond-mat/0501259].

[3] J. M. Maldacena, "The Large N limit of superconformal field theories and supergravity," Int. J. Theor. Phys. **38**, 1113 (1999) [Adv. Theor. Math. Phys. **2**, 231 (1998)] [hep-th/9711200].

[4] S. S. Gubser, I. R. Klebanov, and A. M. Polyakov, "Gauge theory correlators from noncritical string theory," Phys. Lett. B **428**, 105 (1998) [hep-th/9802109].

[5] E. Witten, "Anti-de Sitter space and holography," Adv. Theor. Math. Phys. **2**, 253 (1998) [hep-th/9802150].

[6] M. Ammon and J. Erdmenger, "Gauge/gravity duality : Foundations and applications," Cambridge University Press (2015).

[7] M. Natsuume, "AdS/CFT Duality User Guide," Lect. Notes Phys. **903**, pp.1 (2015) [arXiv:1409.3575 [hep-th]].

[8] J. Zaanen, Y. W. Sun, Y. Liu, and K. Schalm, "Holographic Duality in Condensed Matter Physics," Cambridge University Press (2015).

[9] S. A. Hartnoll, A. Lucas, and S. Sachdev, "Holographic quantum matter," The MIT Press (2018). [arXiv:1612.07324 [hep-th]].

[10] M. Matsumoto and S. Nakamura, "Critical Exponents of Nonequilibrium Phase Transitions in AdS/CFT Correspondence," Phys. Rev. D **98**, no. 10, 106027 (2018) [arXiv:1804.10124 [hep-th]].

[11] T. Imaizumi, M. Matsumoto, and S. Nakamura, "Current-driven tricritical point in large-N_c gauge theory," arXiv:1911.06262 [hep-th].

[12] V. E. Hubeny and M. Rangamani, "A Holographic view on physics out of equilibrium," Adv. High Energy Phys. **2010**, 297916 (2010) [arXiv:1006.3675 [hep-th]].

[13] P. C. Hohenberg and B. I. Halperin, "Theory of dynamic critical phenomena," Rev. Mod. Phys. **49**, 435 (1977).

[14] J. Polchinski, "Dirichlet Branes and Ramond-Ramond charges," Phys. Rev. Lett. **75**, 4724 (1995) [hep-th/9510017].

[15] E. B. Bogomolny, "Stability of Classical Solutions," Sov. J. Nucl. Phys. **24**, 449 (1976).

[16] M. K. Prasad and C. M. Sommerfield, "Exact Classical Solutions for 't Hooft, Monopole and the Julia-Zee Dyon," Phys. Rev. Lett. **35**, 760 (1975).

[17] G. T. Horowitz and A. Strominger, "Black strings and P-branes," Nucl. Phys. B **360**, 197 (1991).

[18] P. Breitenlohner and D. Z. Freedman, "Stability in Gauged Extended Supergravity," Annals Phys. **144**, 249 (1982).

[19] A. Karch and E. Katz, "Adding flavor to AdS / CFT," JHEP **0206**, 043 (2002) [hep-th/0205236].

[20] O. DeWolfe, D. Z. Freedman and H. Ooguri, "Holography and defect conformal field theories," Phys. Rev. D **66**, 025009 (2002) [hep-th/0111135].

[21] A. Karch and A. O'Bannon, "Metallic AdS/CFT," JHEP **09**, 024 (2007) [arXiv:0705.3870 [hep-th]].

[22] N. Nakagawa and S.-i. Sasa, "Liquid-gas transitions in steady heat conduction," Phys. Rev. Lett. **119**, 260602 (2017).

[23] J. Babington, J. Erdmenger, N. J. Evans, Z. Guralnik, and I. Kirsch, "Chiral symmetry breaking and pions in nonsupersymmetric gauge/gravity duals," Phys. Rev. D **69**, 066007 (2004) [hep-th/0306018].

[24] M. Kruczenski, D. Mateos, R. C. Myers, and D. J. Winters, "Towards a holographic dual of large-N_c QCD," JHEP **05**, 041 (2004) [hep-th/0311270].

[25] A. Karch, A. O'Bannon, and K. Skenderis, "Holographic renormalization of probe D-branes in AdS/CFT," JHEP **0604**, 015 (2006) [hep-th/0512125].

[26] T. Albash, V. G. Filev, C. V. Johnson, and A. Kundu, "Quarks in an external electric field in finite temperature large N gauge theory," JHEP **08**, 092 (2008) [arXiv:0709.1554 [hep-th]].

[27] S. Nakamura, "Negative Differential Resistivity from Holography," Prog. Theor. Phys. **124**, 1105 (2010) [arXiv:1006.4105 [hep-th]].

[28] S. Nakamura, "Nonequilibrium Phase Transitions and Nonequilibrium Critical Point from AdS/CFT," Phys. Rev. Lett. **109**, 120602 (2012) [arXiv:1204.1971 [hep-th]].

[29] A. Banerjee, A. Kundu, and S. Kundu, "Flavour Fields in Steady State: Stress Tensor and Free Energy," JHEP **1602**, 102 (2016) [arXiv:1512.05472 [hep-th]].

[30] B. Widom and J. S. Rowlinson, "New model for the study of liquidvapor phase transitions," J. Chem. Phys. **52**, 1670 (1970).

[31] N. D. Mermin, "Lattice Gas with Short-Range Pair Inter- actions and a Singular Coexistence-Curve Diameter," Phys. Rev. Lett. **26**, 957 (1971).

[32] G. Stell and P. C. Hemmer, "Phase transitions due to softness of the potential core," J. Chem. Phys. **56**, 4274 (1972).

[33] J. J. Rehr and N. D. Mermin, "Revised scaling equation of state at the liquid-vapor critical point," Phys. Rev. A **8**, 472 (1973).

[34] J. Mas, J. P. Shock, J. Tarrio, and D. Zoakos, "Holographic Spectral Functions at Finite Baryon Density," JHEP **0809**, 009 (2008) [arXiv:0805.2601 [hep-th]].

[35] J. Mas, J. P. Shock, and J. Tarrio, "Holographic Spectral Functions in Metallic AdS/CFT," JHEP **0909**, 032 (2009) [arXiv:0904.3905 [hep-th]].

[36] D. T. Son and A. O. Starinets, "Minkowski space correlators in AdS / CFT correspondence: Recipe and applications," JHEP **0209**, 042 (2002) [hep-th/0205051].

[37] M. Ammon, T. H. Ngo, and A. O'Bannon, "Holographic Flavor Transport in Arbitrary Constant Background Fields," JHEP **0910**, 027 (2009) [arXiv:0908.2625 [hep-th]].

[38] M. Ali-Akbari and A. Vahedi, "Non-equilibrium Phase Transition from AdS/CFT," Nucl. Phys. B **877**, 95 (2013) [arXiv:1305.3713 [hep-th]].

[39] J. Babington, J. Erdmenger, N. J. Evans, Z. Guralnik, and I. Kirsch, "Chiral symmetry breaking and pions in nonsupersymmetric gauge / gravity duals," Phys. Rev. D **69**, 066007 (2004) [hep-th/0306018].

[40] V. G. Filev, C. V. Johnson, R. C. Rashkov, and K. S. Viswanathan, "Flavoured large N gauge theory in an external magnetic field," JHEP **0710**, 019 (2007) [hep-th/0701001].

[41] T. Albash, V. G. Filev, C. V. Johnson, and A. Kundu, "Finite temperature large N gauge theory with quarks in an external magnetic field," JHEP **0807**, 080 (2008) [arXiv:0709.1547 [hep-th]].

[42] V. G. Filev, "Criticality, scaling and chiral symmetry breaking in external magnetic field," JHEP **0804**, 088 (2008) [arXiv:0706.3811 [hep-th]].

[43] J. Erdmenger, R. Meyer, and J. P. Shock, "AdS/CFT with flavour in electric and magnetic Kalb-Ramond fields," JHEP **0712**, 091 (2007) [arXiv:0709.1551 [hep-th]].

[44] A. M. Halasz, A. D. Jackson, R. E. Shrock, M. A. Stephanov, and J. J. M. Verbaarschot, "On the phase diagram of QCD," Phys. Rev. D **58**, 096007 (1998) [hep-ph/9804290].

[45] R. C. Myers, A. O. Starinets, and R. M. Thomson, "Holographic spectral functions and diffusion constants for fundamental matter," JHEP **0711**, 091 (2007) [arXiv:0706.0162 [hep-th]].

[46] C.Hoyos-Badajoz, K.Landsteiner and S.Montero, "Holographic meson melting," JHEP **0704**, 031 (2007) [hep-th/0612169].